Pergamon

Int. J. Solids Structures Vol. 31, No. 11, pp. 1609–1631, 1994
Elsevier Science Ltd
Printed in Great Britain
0020–7683/94 $7.00 + .00

0020–7683(93)E0031–C

EXACT ANALYTICAL SOLUTIONS FOR FREE VIBRATIONS OF THICK SECTORIAL PLATES WITH SIMPLY SUPPORTED RADIAL EDGES

C. S. HUANG† and O. G. MCGEE‡
Department of Civil Engineering, The Ohio State University, Columbus, Ohio, U.S.A.

and

A. W. LEISSA
Department of Engineering Mechanics, The Ohio State University, Columbus, Ohio, U.S.A.

(*Received* 3 *February* 1993)

Abstract—The first known exact analytical solutions are derived for the free vibrations of thick (Mindlin) sectorial plates having simply supported radial edges and arbitrary conditions along the circular edge. The general solutions to the Mindlin differential equations of motion contain non-integer order ordinary and modified Bessel functions of the first and second kinds, and six arbitrary constants of integration. By exercising a careful limiting process, three regularity conditions at the vertex of the radial edges are invoked to yield three equations of constraint among the six constants for sector angles exceeding 180° (re-entrant corners). Three additional linearly independent equations among the six constants are obtained by satisfying the three boundary conditions along the circular edge. Frequency determinant equations are derived for Mindlin sectorial plates with circular boundaries which are clamped, simply supported, or free. Nondimensional frequency parameters are presented for over a wide range of salient and re-entrant sector angles ($30° \leqslant \alpha \leqslant 360°$), and thickness-to-radius ratios of 0.1, 0.2 and 0.4. Frequency results obtained for Mindlin sectorial plates are compared to those determined for classically thin sectorial plates, and the results are found to be considerably different than those derived from thin plate theory, particularly for the fundamental frequencies of plates having sector angles slightly greater than 180° when the circular boundary is free. The frequencies for 360° sectorial plates (i.e. circular plates having a hinged crack) are compared with those for complete circular ones.

INTRODUCTION

Quite literally hundreds of published references exist (Leissa, 1969, 1977, 1981, 1987) on the free vibrations of complete circular and annular, thin and thick plates (with no radial boundaries). However, the scope of previous work done for the sectorial plate (see Fig. 1) is narrow. Several authors have offered approximate theoretical and experimental vibration data for thin sectorial plates with various edge conditions on the circular and radial edges, namely Ben-Amoz (1959), Westmann (1962), Bhattacharya and Bhowmic (1975), Rubin (1975) and Maruyama and Ichinomiya (1981). Bapu Rao *et al.* (1977) and Guruswamy and Yang (1979) proposed various Reissner sector plate finite element formulations for approximate vibration analysis of thick circular and annular sectorial plates. Cheung and Chan (1981) offered a three-dimensional curved finite strip method for static and vibration analyses of thin and thick sectorial plates with arbitrary conditions on the circular and radial edges. Srinivasan and Thiruvenkatachari (1985) reported natural frequencies of moderately thick Mindlin annular sector plates with clamped circular and radial edges.

The customary form of the exact analytical solutions for free vibrations of complete circular thin plates with arbitrary boundary conditions are appropriate to sectorial thin plates with simply supported radial edges (Leissa, 1969). These solutions involve non-integer order Bessel functions of the first and second kinds and two constants of integration, since the modified Bessel functions of the first and second kinds are omitted to eradicate all singularities at the plate origin ($r = 0$). Recent work by the present authors (Leissa *et al.*, 1992) advocates that use of the ordinary Bessel functions solution is incorrect for

† Current address: National Center for Research on Earthquake Engineering (NCREE), National Taiwan University, Taipei, Taiwan, R.O.C.
‡ Current address: School of Civil and Environmental Engineering, Georgia Institute of Technology, Atlanta, Georgia, U.S.A.

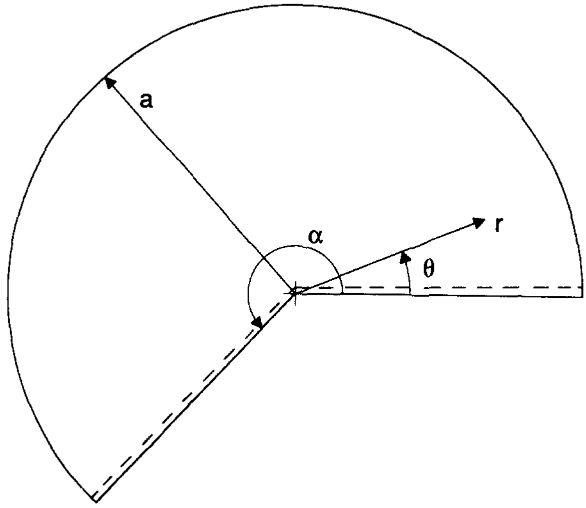

Fig. 1. A thick sectorial plate with simply supported radial edges forming a re-entrant corner ($\alpha > 180°$).

sectorial thin plates having simply supported radial edges and sector angle, $\alpha > 180°$ (forming a re-entrant corner, see Fig. 1). In this configuration, the singular vibratory bending moment at the re-entrant corner is improperly represented by this solution. Nonetheless, this work (Leissa *et al.*, 1992a) does present some approximate, yet highly accurate, vibration results for sectorial thin plates with $\alpha > 180°$. These results were obtained by means of the Ritz method, using corner functions to represent the thin plate singularities properly at $r = 0$.

A subsequent paper by the present authors (Huang *et al.*, 1992) documents the first known exact analytical solutions for the free vibrations of sectorial thin plates having simply supported radial edges forming re-entrant corners ($\alpha > 180°$) and arbitrary circular edge conditions. The solutions therein involve non-integer order ordinary and modified Bessel functions of the first and second kinds, and four constants of integration. In the present paper the above analytical procedure is extended to the flexural vibrations of Mindlin sectorial plates having simply supported radial edges forming re-entrant corners. The Mindlin simply supported radial edge conditions are defined such that the transverse displacement, circumferential moment, and tangential rotation all vanish. The Mindlin sectorial plates call for a Bessel function solution analogous to the classically thin plates, but with six, instead of four, constants of integration. The analytical procedure requires satisfying (i) the Mindlin differential equations of motion, (ii) the nine boundary conditions along the radial and circular edges, and (iii) the three regularity conditions at the vertex of the radial edges.

Frequency determinant equations are derived for Mindlin sectorial plates with circular boundaries which are clamped, simply supported, or free. Nondimensional frequency parameters are presented for each of these plate configurations over a wide range of sector angles (α), including re-entrant ones, and thickness-to-radius ratios (h/a) (see Fig. 1). The singularities in the vibratory bending moments and shear forces at the vertex of Mindlin sectorial plates are also identified.

EXACT SOLUTION

Consider in Fig. 1 the homogeneous, isotropic sectorial plate of thickness h (not shown), with polar coordinates (r, θ) at the midplane. The vibratory displacements (u_r, u_θ, w) of the midplane are assumed as

$$\begin{aligned} u_r &= z\Psi_r(r, \theta, t) \\ u_\theta &= z\Psi_\theta(r, \theta, t) \\ w &= w(r, \theta, t), \end{aligned} \tag{1}$$

where u_r and u_θ are components parallel to the midplane, w is transverse, t is time, and Ψ_r and Ψ_θ are the bending rotations of the midplane normal in the radial and circumferential directions, respectively. The equations of motion in terms of stress resultants in polar coordinates are (cf. Mindlin and Deresiewicz, 1954)

$$\begin{aligned}\partial M_r/\partial r+r^{-1}\,\partial M_{r\theta}/\partial\theta+r^{-1}(M_r-M_\theta)-Q_r &= (\rho h^3/12)\,\partial^2\Psi_r/\partial t^2\\ \partial M_{r\theta}/\partial r+r^{-1}\,\partial M_\theta/\partial\theta+2r^{-1}(M_{r\theta})-Q_\theta &= (\rho h^3/12)\,\partial^2\Psi_\theta/\partial t^2\\ \partial Q_r/\partial r+r^{-1}\,\partial Q_\theta/\partial\theta+r^{-1}(Q_r) &= r\rho h\,\partial^2 w/\partial t^2,\end{aligned} \tag{2}$$

where ρ is the mass density per unit volume. The stress resultants (moments and shears) are related to the transverse displacement and bending rotations by

$$M_r = D[\partial\Psi_r/\partial r+\nu r^{-1}(\Psi_r+\partial\Psi_\theta/\partial\theta)] \tag{3a}$$

$$M_\theta = D[r^{-1}(\Psi_r+\partial\Psi_\theta/\partial\theta)+\nu\,\partial\Psi_r/\partial r] \tag{3b}$$

$$M_{r\theta} = [(1-\nu)/2]\cdot D[r^{-1}(\partial\Psi_r/\partial\theta-\Psi_\theta)+\partial\Psi_\theta/\partial r] \tag{3c}$$

$$Q_r = \kappa^2 Gh(\Psi_r+\partial w/\partial r) \tag{3d}$$

$$Q_\theta = \kappa^2 Gh(\Psi_\theta+r^{-1}\,\partial w/\partial\theta), \tag{3e}$$

where $D = Eh^3/12(1-\nu^2)$ is the flexural rigidity, E is the modulus of elasticity, ν is Poisson's ratio, $\kappa^2 = \pi^2/12$ is the shear correction factor, and G is the shear modulus. Assuming first a sinusoidal motion in time

$$\begin{aligned}\Psi_r(r,\theta,t) &= \psi_r(r,\theta)\cos\omega t\\ \Psi_\theta(r,\theta,t) &= \psi_\theta(r,\theta)\cos\omega t\\ w_r(r,\theta,t) &= W(r,\theta)\cos\omega t\end{aligned} \tag{4}$$

then eqns (2) become

$$\begin{aligned}\partial M_r/\partial r+r^{-1}\,\partial M_{r\theta}/\partial\theta+r^{-1}(M_r-M_\theta)-Q_r+(\omega^2\rho h^3/12)\psi_r &= 0\\ \partial M_{r\theta}/\partial r+r^{-1}\,\partial M_\theta/\partial\theta+2r^{-1}(M_{r\theta})-Q_\theta+(\omega^2\rho h^3/12)\psi_\theta &= 0\\ \partial Q_r/\partial r+r^{-1}\,\partial Q_\theta/\partial\theta+r^{-1}(Q_r)+\omega^2\rho hW &= 0.\end{aligned} \tag{5}$$

The transverse deflection (W) and the angular rotations (ψ_r and ψ_θ) are defined in terms of three potential functions ϕ_1, ϕ_2 and ϕ_3 (Mindlin and Deresiewicz, 1954), as follows:

$$\psi_r = (\sigma_1-1)\,\partial\phi_1/\partial r+(\sigma_2-1)\,\partial\phi_2/\partial r+r^{-1}\,\partial\phi_3/\partial\theta \tag{6a}$$

$$\psi_\theta = (\sigma_1-1)r^{-1}\,\partial\phi_1/\partial\theta+(\sigma_2-1)r^{-1}\,\partial\phi_2/\partial\theta-\partial\phi_3/\partial r \tag{6b}$$

$$W = \phi_1+\phi_2, \tag{6c}$$

where the following dimensionless parameters have been introduced

$$\sigma_1,\sigma_2 = (\delta_2^2,\delta_1^2)(R\lambda^4-S^{-1})^{-1} \tag{7}$$

$$\delta_1^2,\delta_2^2 = (\lambda^4/2)\{R+S\pm[(R-S)^2+4\lambda^{-4}]^{1/2}\} \tag{8}$$

$$R = h^2/12,\quad S = D/(\kappa^2 Gh),\quad \lambda^4 = \rho\omega^2 h/D. \tag{9}$$

Substituting eqns (3) and (6) into (5), three Laplace equations in ϕ_1, ϕ_2 and ϕ_3 are the result after some algebraic manipulations

$$(\nabla^2+\delta_1^2)\phi_1 = 0$$
$$(\nabla^2+\delta_2^2)\phi_2 = 0$$
$$(\nabla^2+\delta_3^2)\phi_3 = 0, \tag{10}$$

where ∇^2 is the harmonic differential operator, and

$$\delta_3^2 = 2(R\lambda^4 - S^{-1})/(1-\nu). \tag{11}$$

The solution of eqns (5) requires finding the potential functions, ϕ_1, ϕ_2 and ϕ_3 that satisfy eqns (10).

It is interesting that the literature documents considerable discrepancies in the use of the transformation eqns (6)–(9), first proposed by Mindlin and Deresiewicz (1954), and subsequently used by Irie *et al.* (1979, 1980, 1982). The expressions for δ_1 and δ_2 used in the analytical formulation of Callahan (1955) and in the numerical calculations of Rao and Prasad (1975) not only differ from each other, but they indeed do not make eqn (6) satisfy the equations of motion [eqns (5)]. Consequently, by using these incorrect transformation equations, free vibration results calculated for circular, annular, and sectorial plates are erroneously too stiff as the plate thickness is increased, as pointed out by Irie *et al.* (1979, 1980, 1982).

Utilizing the polar coordinates of Fig. 1, it is assumed that

$$\phi_1(r,\theta) = R_{n_1}\sin(n\pi\theta/\alpha) \tag{12a}$$

$$\phi_2(r,\theta) = R_{n_2}\sin(n\pi\theta/\alpha) \tag{12b}$$

$$\phi_3(r,\theta) = R_{n_3}\cos(n\pi\theta/\alpha) \tag{12c}$$

with $n = 1,2,3,\ldots$. This results in the satisfaction of the simply supported boundary conditions along $\theta = 0$ and $\theta = \alpha$ exactly. That is

$$W(r,0) = W(r,\alpha) = 0 \tag{13a}$$

$$M_\theta(r,0) = M_\theta(r,\alpha) = 0 \tag{13b}$$

$$\psi_r(r,0) = \psi_r(r,\alpha) = 0. \tag{13c}$$

Then, from eqn (3c), $M_{r\theta}$ is nonzero along the radial edges. This is essential, otherwise finding suitable displacement functions such as those in eqns (12) is prohibitive. Substituting eqns (12) and considering the linear independence among $\sin(n\pi\theta/\alpha)$ and $\cos(n\pi\theta/\alpha)$ for different n, eqns (10) become

$$r^2R''_{n_i}+rR'_{n_i}+(\delta_i^2r^2-\mu^2)R_{n_i} = 0, \quad i = 1,2,3, \tag{14}$$

where the primes indicate derivatives, and $\mu = n\pi/\alpha$ is positive and is typically non-integer.

Generally speaking, the solutions to eqns (14) involve ordinary and/or modified Bessel functions of the first and second kinds (depending upon the signs of the δ_i^2), and six constants of integration. Six linearly independent equations must be written among the integration constants to solve the title free vibration problem. The three boundary conditions along the circular edge of the Mindlin sectorial plate leads to three of the six equations. Three regularity conditions at $r = 0$ must be enforced to generate three additional equations among the integration constants. These regularity conditions are

$$W_{(r\Rightarrow 0)} = 0 \tag{15a}$$

$$\psi_{r_{(r\Rightarrow 0)}} = \text{finite} \tag{15b}$$

$$\psi_{\theta_{(r\Rightarrow 0)}} = \text{finite}. \tag{15c}$$

In eqns (8) and (11), δ_2^2 and δ_3^2 can be either positive or negative, while δ_1^2 is always positive. Two cases are pertinent to obtaining solutions to eqns (14): $\delta_1^2 > 0$, $\delta_2^2 < 0$, $\delta_3^2 < 0$ and $\delta_1^2 > 0$, $\delta_2^2 > 0$, $\delta_3^2 > 0$. By carefully investigating eqns (8) and (11), one is able to find that δ_2^2 must have the same sign as δ_3^2, that is, either positive or negative, while δ_1^2 is always positive.

Case I: $\delta_1^2 > 0$, $\delta_2^2 < 0$, $\delta_3^2 < 0$ ($\lambda^4 < 1/\mathrm{RS}$)

In this case, the solutions of eqns (14) are

$$R_{n_1}(r) = A_{n_1} J_\mu(\delta_1 r) + B_{n_1} Y_\mu(\delta_1 r) \tag{16a}$$

$$R_{n_2}(r) = A_{n_2} I_\mu(\delta_2 r) + B_{n_2} K_\mu(\delta_2 r) \tag{16b}$$

$$R_{n_3}(r) = A_{n_3} I_\mu(\delta_3 r) + B_{n_3} K_\mu(\delta_3 r), \tag{16c}$$

where J_μ, Y_μ, I_μ and K_μ are ordinary and modified Bessel functions of the first and second kinds, and A_{n_i} and B_{n_i} ($i = 1, 2, 3$) are arbitrary constants of integration. Equations (16) are the same as the classical solution used for complete circular Mindlin plates, except that (1) μ is not, in general, an integer, and (2) B_{n_1}, B_{n_2} and B_{n_3} are not necessarily set equal to zero.

Considering now the displacement condition given by eqn (15a), since

$$J_\mu(0) = I_\mu(0) = 0, \quad \mu > 0 \tag{17}$$

then, by using eqn (6c), eqn (15a) becomes

$$\lim_{r\Rightarrow 0} [B_{n_1} Y_\mu(\delta_1 r) + B_{n_2} K_\mu(\delta_2 r)] = 0. \tag{18}$$

The Bessel functions of the second kind may be expressed as (cf. Tranter, 1968)

$$Y_\mu(\delta r) = [\cos \mu\pi \cdot J_\mu(\delta r) - J_{-\mu}(\delta r)] \cdot (\sin \mu\pi)^{-1} \tag{19a}$$

$$K_\mu(\delta r) = -[I_\mu(\delta r) - I_{-\mu}(\delta r)] \cdot (\pi/2)(\sin \pi\mu)^{-1}. \tag{19b}$$

By using eqns (17) and (19), eqn (18) is reduced to

$$\lim_{r\Rightarrow 0} [-B_{n_1} J_{-\mu}(\delta_1 r) + (\pi/2) B_{n_2} I_{-\mu}(\delta_2 r)] = 0. \tag{20}$$

The Bessel functions may be expressed in terms of their power series

$$J_{-\mu}(\delta r) = \sum_{j=0,1}^{\infty} \frac{(-1)^j (\delta r/2)^{-\mu+2j}}{j!\Gamma(-\mu+j+1)} \tag{21a}$$

$$I_{-\mu}(\delta r) = \sum_{j=0,1}^{\infty} \frac{(\delta r/2)^{-\mu+2j}}{j!\Gamma(-\mu+j+1)}, \tag{21b}$$

where Γ is the gamma function. By substituting eqns (21) into (20), the resulting limit is satisfied when the coefficients of r with degree $-\mu+2j$ less than or equal to zero vanish, because B_{n_1} and B_{n_2} are finite. That is

$$-(-1)^j\delta_1^{-\mu+2j}B_{n_1}+(\pi/2)\delta_2^{-\mu+2j}B_{n_2}=0,\quad -\mu+2j\leqslant 0;\quad j=0,1,2,\ldots. \tag{22}$$

Indeed, $\mu>2$ results in $B_{n_1}=B_{n_2}=0$, because in this case eqn (22) generates more than one linearly independent homogeneous equation.

Using eqn (6a), the first rotation regularity condition given by eqn (15b) results in

$$\begin{aligned}\lim_{r\Rightarrow 0}[(\sigma_1-1)[A_{n_1}\delta_1J'_\mu(\delta_1r)+B_{n_1}\delta_1Y'_\mu(\delta_1r)]\\ +(\sigma_2-1)[A_{n_2}\delta_2I'_\mu(\delta_2r)+B_{n_2}\delta_2K'_\mu(\delta_2r)]\\ -(\mu/r)[A_{n_3}I_\mu(\delta_3r)+B_{n_3}K_\mu(\delta_3r)]]=\text{finite}.\end{aligned} \tag{23}$$

The derivatives of the Bessel functions may be expressed as (cf. Tranter, 1968)

$$\begin{aligned}2J'_\mu(\delta r)&=J_{\mu-1}(\delta r)-J_{\mu+1}(\delta r)\\ 2Y'_\mu(\delta r)&=Y_{\mu-1}(\delta r)-Y_{\mu+1}(\delta r)\\ 2I'_\mu(\delta r)&=I_{\mu-1}(\delta r)+I_{\mu+1}(\delta r)\\ 2K'_\mu(\delta r)&=-K_{\mu-1}(\delta r)-K_{\mu+1}(\delta r).\end{aligned} \tag{24}$$

Using eqns (17) and (19), one obtains the following when eqns (24) are substituted into eqn (23)

$$\begin{aligned}&\lim_{r\Rightarrow 0}[(\sigma_1-1)(\delta_1/2)(A_{n_1}J_{\mu-1}(\delta_1r)+B_{n_1}([\sin(\mu-1)\pi]^{-1}[\cos(\mu-1)\pi\\ &\quad\cdot J_{\mu-1}(\delta_1r)-J_{-\mu+1}(\delta_1r)]+[\sin(\mu+1)\pi]^{-1}J_{-\mu-1}(\delta_1r)))\\ &\quad+(\sigma_2-1)(\delta_2/2)(A_{n_2}I_{\mu-1}(\delta_2r)-B_{n_2}((\pi/2)[\sin(\mu-1)\pi]^{-1}\\ &\quad\cdot[I_{-\mu+1}(\delta_2r)-I_{\mu-1}(\delta_2r)]+[\sin(\mu+1)\pi]^{-1}I_{-\mu-1}(\delta_2r)))\\ &\quad-(\mu/r)(A_{n_3}I_\mu(\delta_3r)+B_{n_3}(\pi/2)[\sin\mu\pi]^{-1}[I_{-\mu}(\delta_3r)-I_\mu(\delta_3r)])]=\text{finite}.\end{aligned} \tag{25}$$

This yields, upon substituting eqns (21)

$$\begin{aligned}&\lim_{r\Rightarrow 0}\sum_{j=0,1}^{\infty}[(\sigma_1-1)(A_{n_1}(\delta_1/2)(-1)^j(\delta_1r/2)^{\mu+2j-1}\cdot[j!\Gamma(\mu+j)]^{-1}\\ &\quad+B_{n_1}(\delta_1/2)([\cos(\mu-1)\pi]\cdot[\sin(\mu-1)\pi]^{-1}\cdot[(-1)^j(\delta_1r/2)^{\mu+2j-1}]\\ &\quad\cdot[j!\Gamma(\mu+j)]^{-1}-[\sin(\mu-1)\pi]^{-1}\cdot[(-1)^j(\delta_1r/2)^{-\mu+2j+1}]\cdot[j!\Gamma(-\mu+j+2)]^{-1}\\ &\quad+[\sin(\mu+1)\pi]^{-1}\cdot[(-1)^j(\delta_1r/2)^{-\mu+2j-1}]\cdot[j!\Gamma(-\mu+j)]^{-1}))\\ &\quad+(\sigma_2-1)(A_{n_2}(\delta_2/2)(\delta_2r/2)^{\mu+2j-1}\cdot[j!\Gamma(\mu+j)]^{-1}\\ &\quad-B_{n_2}(\pi\delta_2/4)([\sin(\mu-1)\pi]^{-1}\cdot(\delta_2r/2)^{-\mu+2j+1}\cdot[j!\Gamma(-\mu+j+2)]^{-1}\\ &\quad-[\sin(\mu-1)\pi]^{-1}\cdot(\delta_2r/2)^{\mu+2j-1}\cdot[j!\Gamma(\mu+j)]^{-1}\\ &\quad+[\sin(\mu+1)\pi]^{-1}\cdot(\delta_2r/2)^{-\mu+2j-1}\cdot[j!\Gamma(-\mu+j)]^{-1}))\\ &\quad-(\mu/r)(A_{n_3}(\delta_3r/2)^{\mu+2j}\cdot[j!\Gamma(\mu+j+1)]^{-1}\\ &\quad+B_{n_3}(\pi/2)(\sin\mu\pi)^{-1}((\delta_3r/2)^{-\mu+2j}\cdot[j!\Gamma(-\mu+j+1)]^{-1}\\ &\quad-(\delta_3r/2)^{\mu+2j}\cdot[j!\Gamma(\mu+j+1)]^{-1}))]=\text{finite}.\end{aligned} \tag{26}$$

Because A_{n_i} and B_{n_i} $(i=1,2,3)$ are finite, satisfaction of eqn (26) requires that the coefficients of r with power less than zero vanish. To clarify the analysis without loss of generality, the range of μ is assessed in the subintervals $0<\mu<1$, $1<\mu<2$ and $\mu>2$.

Subcase I(a) : $0 < \mu < 1$. In this range, all terms in eqn (26) vanish in the limit, except those for $j = 0$. The remaining terms contain $r^{\mu-1}$ and $r^{-\mu-1}$. From the coefficients of $r^{-\mu-1}$

$$((\sigma_1-1)(\delta_1/2)^{-\mu}\cdot[\Gamma(-\mu)\cdot\sin(\mu+1)\pi]^{-1})B_{n_1}$$
$$-((\sigma_2-1)(\pi/2)(\delta_2/2)^{-\mu}\cdot[\Gamma(-\mu)\cdot\sin(\mu+1)\pi]^{-1})B_{n_2}$$
$$-((\pi\mu/2)(\delta_3/2)^{-\mu}\cdot[\Gamma(1-\mu)\cdot\sin\mu\pi]^{-1})B_{n_3}=0. \quad (27)$$

Since $\sin(\mu+1)\pi = -\sin\mu\pi$ and $\Gamma(-\mu+1) = -\mu\Gamma(-\mu)$, one can simplify eqn (27) to

$$(\sigma_1-1)\delta_1^{-\mu}B_{n_1}-(\pi/2)(\sigma_2-1)\delta_2^{-\mu}B_{n_2}-(\pi/2)\delta_3^{-\mu}B_{n_3}=0. \quad (28)$$

From the coefficients of $r^{\mu-1}$

$$((\sigma_1-1)(\delta_1/2)^{\mu}[\Gamma(\mu)]^{-1})A_{n_1}+((\sigma_1-1)\cdot\cot(\mu-1)\pi\cdot(\delta_1/2)^{\mu}[\Gamma(\mu)]^{-1})B_{n_1}$$
$$+((\sigma_2-1)(\delta_2/2)^{\mu}[\Gamma(\mu)]^{-1})A_{n_2}+((\sigma_2-1)\cdot\pi/[2\sin(\mu-1)\pi]\cdot(\delta_2/2)^{\mu}[\Gamma(\mu)]^{-1})B_{n_2}$$
$$-(\mu(\delta_3/2)^{\mu}[\Gamma(\mu+1)]^{-1})A_{n_3}+(\pi\mu/[2\sin\mu\pi]\cdot(\delta_3/2)^{\mu}[\Gamma(\mu+1)]^{-1})B_{n_3}=0. \quad (29)$$

Since $\sin(\mu-1)\pi = -\sin\mu\pi$ and $\Gamma(\mu+1) = \mu\Gamma(\mu)$, one can also reduce eqn (29) to

$$(\sigma_1-1)\delta_1^{\mu}A_{n_1}+(\sigma_1-1)\cdot\cot\mu\pi\cdot\delta_1^{\mu}B_{n_1}+(\sigma_2-1)\delta_2^{\mu}A_{n_2}$$
$$-(\sigma_2-1)\cdot\pi/[2\sin\mu\pi]\cdot\delta_2^{\mu}B_{n_2}-\delta_3^{\mu}A_{n_3}+\pi/[2\sin\mu\pi]\cdot\delta_3^{\mu}B_{n_3}=0. \quad (30)$$

From eqn (22), the following relation is applicable

$$B_{n_1}=\pi/2\cdot(\delta_1/\delta_2)^{\mu}B_{n_2} \quad (31)$$

and substituting eqn (31) into (28), one sees that

$$B_{n_3}=(\sigma_1-\sigma_2)(\delta_3/\delta_2)^{\mu}B_{n_2}. \quad (32)$$

When eqns (31) and (32) are used in eqn (30), the latter simplifies to

$$(\sigma_1-1)\delta_1^{\mu}A_{n_1}+(\sigma_2-1)\delta_2^{\mu}A_{n_2}+\pi/[2\sin\mu\pi]\cdot\delta_2^{-\mu}((\sigma_1-1)\cdot\cos\mu\pi\cdot\delta_1^{2\mu}$$
$$-(\sigma_2-1)\delta_2^{2\mu}+(\sigma_1-\sigma_2)\delta_3^{2\mu})B_{n_2}-\delta_3^{\mu}A_{n_3}=0. \quad (33)$$

Subcase I(b) : $1 < \mu < 2$. In this range, all terms in eqn (26) vanish as r approaches zero, except those terms containing $r^{-\mu+2j+1}$ for $j = 0$, and $r-\mu+2j-1$ for $j = 0$ and $j = 1$. The remaining terms contain $r^{-\mu+1}$ and $r^{-\mu-1}$. In the limit, the coefficients of $r^{-\mu-1}$ yield eqn (28). From the coefficients of $r^{-\mu+1}$

$$(\sigma_1-1)(-(\delta_1/2)^{-\mu+2}\cdot[\Gamma(-\mu+2)\cdot\sin(\mu-1)\pi]^{-1}$$
$$-(\delta_1/2)^{-\mu+2}\cdot[\Gamma(-\mu+1)\cdot\sin(\mu+1)\pi]^{-1})B_{n_1}$$
$$-(\sigma_2-1)\cdot\pi/2((\delta_2/2)^{-\mu+2}\cdot[\Gamma(-\mu+2)\cdot\sin(\mu-1)\pi]^{-1}$$
$$+(\delta_2/2)^{-\mu+2}\cdot[\Gamma(-\mu+1)\cdot\sin(\mu-1)\pi]^{-1})B_{n_2}$$
$$+((\pi\mu/2)(\delta_3/2)^{-\mu+2}\cdot[\Gamma(-\mu+2)\cdot\sin\mu\pi]^{-1})B_{n_3}=0. \quad (34)$$

Using $\sin(\mu-1)\pi = -\sin\mu\pi$ and $\Gamma(-\mu+1) = (-\mu+1)\Gamma(-\mu+1)$, eqn (34) simplifies to

$$(\sigma_1-1)(-\mu+2)\delta_1^{-\mu+2}B_{n_1}+(\sigma_2-1)(-\mu+2)(\pi/2)\delta_2^{-\mu+2}B_{n_2}+(\mu\pi/2)\delta_3^{-\mu+2}B_{n_3}=0. \quad (35)$$

The three linearly independent homogeneous equations (22), (28) and (35) result in $B_{n_1} = B_{n_2} = B_{n_3} = 0$.

Details of addressing the last regularity condition [eqn (15c)] are given in Appendix A. The results there are exactly the same relations obtained from satisfying eqn (15b); that is, eqns (A4) and (A6) are identical to eqns (28) and (30), respectively; and eqns (A4), (A8) and (22) result in $B_{n_1} = B_{n_2} = B_{n_3} = 0$.

Subcase I(c): $\mu > 2$. In this range, one finds that eqns (22) and (28) resolve to $B_{n_1} = B_{n_2} = B_{n_3} = 0$. Similarly, for integer values of μ, it can be proven that $B_{n_1} = B_{n_2} = B_{n_3} = 0$. The latter proof can be easily realized by using equations analogous to eqns (19) and (21), but for Bessel functions of integer order.

Case II: $\delta_1^2 > 0$, $\delta_2^2 > 0$, $\delta_3^2 > 0$ ($\lambda^4 > 1/\mathrm{RS}$)

In this case, the solutions of eqns (14) are

$$R_{n_i}(r) = A_{n_i} J_\mu(\delta_i r) + B_{n_i} Y_\mu(\delta_i r), \quad i = 1, 2, 3. \tag{36}$$

From the regularity condition on the transverse displacement [eqn (15a)], the following relation is derived by using eqns (17) and (19a)

$$\lim_{r \Rightarrow 0} [-B_{n_1} J_{-\mu}(\delta_1 r) - B_{n_2} J_{-\mu}(\delta_2 r)] = 0. \tag{37}$$

Assuming B_{n_1} and B_{n_2} are finite and using eqn (21a), the limit eqn (37) yields

$$\delta_1^{-\mu+2j} B_{n_1} + \delta_2^{-\mu+2j} B_{n_2} = 0, \quad -\mu + 2j \leqslant 0; j = 0, 1, 2, \ldots. \tag{38}$$

The regularity condition [eqn (15b)] results in

$$\begin{aligned} \lim_{r \Rightarrow 0} [(\sigma_1 - 1)\delta_1 [A_{n_1} J'_\mu(\delta_1 r) + B_{n_1} Y'_\mu(\delta_1 r)] \\ + (\sigma_2 - 1)\delta_2 [A_{n_2} J'_\mu(\delta_2 r) + B_{n_2} Y'_\mu(\delta_2 r)] \\ - (\mu/r)[A_{n_3} J_\mu(\delta_3 r) + B_{n_3} Y_\mu(\delta_3 r)]] = \text{finite}. \end{aligned} \tag{39}$$

Using eqns (17), (19), (21) and (24), eqn (39) becomes

$$\begin{aligned} \lim_{r \Rightarrow 0} \sum_{j=0,1}^{\infty} [(\sigma_1 - 1)(A_{n_1}(\delta_1/2)(-1)^j(\delta_1 r/2)^{\mu+2j-1} \cdot [j!\Gamma(\mu+j)]^{-1} \\ + B_{n_1}(\delta_1/2)([\cos(\mu-1)\pi] \cdot [\sin(\mu-1)\pi]^{-1} \cdot [(-1)^j(\delta_1 r/2)^{\mu+2j-1}] \\ \cdot [j!\Gamma(\mu+j)]^{-1} - [\sin(\mu-1)\pi]^{-1} \cdot [(-1)^j(\delta_1 r/2)^{-\mu+2j+1}] \cdot [j!\Gamma(-\mu+j+2)]^{-1} \\ + [\sin(\mu+1)\pi]^{-1} \cdot [(-1)^j(\delta_1 r/2)^{-\mu+2j-1}] \cdot [j!\Gamma(-\mu+j)]^{-1})) \\ + (\sigma_2 - 1)(A_{n_2}(\delta_2/2)(-1)^j(\delta_2 r/2)^{\mu+2j-1} \cdot [j!\Gamma(\mu+j)]^{-1} \\ + B_{n_2}(\delta_2/2)([\cos(\mu-1)\pi] \cdot [\sin(\mu-1)\pi]^{-1} \cdot [(-1)^j(\delta_2 r/2)^{\mu+2j-1}] \\ \cdot [j!\Gamma(\mu+j)]^{-1} - [\sin(\mu-1)\pi]^{-1} \cdot [(-1)^j(\delta_2 r/2)^{-\mu+2j+1}] \cdot [j!\Gamma(-\mu+j+2)]^{-1} \\ + [\sin(\mu+1)\pi]^{-1} \cdot [(-1)^j(\delta_2 r/2)^{-\mu+2j-1}] \cdot [j!\Gamma(-\mu+j)]^{-1})) \\ - (\mu/r)(A_{n_3}[(-1)^j(\delta_3 r/2)^{\mu+2j}] \cdot [j!\Gamma(\mu+j+1)]^{-1} \\ + B_{n_3}((\cos\mu\pi)(\sin\mu\pi)^{-1}[(-1)^j(\delta_3 r/2)^{\mu+2j}] \cdot [j!\Gamma(\mu+j+1)]^{-1} \\ - (\sin\mu\pi)^{-1}[(-1)^j(\delta_3 r/2)^{-\mu+2j}] \cdot [j!\Gamma(-\mu+j+1)]^{-1}))] = \text{finite}. \end{aligned} \tag{40}$$

Because A_{n_i} and B_{n_i} $(i = 1, 2, 3)$ are finite, satisfaction of eqn (40) requires that the coefficients of r with power less than zero vanish. As outlined previously, the range of μ are considered in the subintervals $0 < \mu < 1$ and $1 < \mu < 2$.

Subcase II(a) : $0 < \mu < 1$. In this range, all terms in eqn (40) vanish in the limit, except those for $j = 0$. While the coefficients of $r^{-\mu-1}$ suggest that

$$(\sigma_1 - 1)\delta_1^{-\mu} B_{n_1} + (\sigma_2 - 1)\delta_2^{-\mu} B_{n_2} + \delta_3^{-\mu} B_{n_3} = 0, \tag{41}$$

the coefficients of $r^{\mu-1}$ require that

$$(\sigma_1 - 1)\delta_1^{\mu} A_{n_1} + (\sigma_1 - 1)\cdot\cos\mu\pi\cdot\delta_1^{\mu} B_{n_1} + (\sigma_2 - 1)\delta_2^{\mu} A_{n_2} \\ + (\sigma_2 - 1)\cdot\cot\mu\pi\cdot\delta_2^{\mu} B_{n_2} - \delta_3^{\mu} A_{n_3} - \cot\mu\pi\cdot\delta_3^{\mu} B_{n_3} = 0. \tag{42}$$

From eqn (38)

$$B_{n_1} = -(\delta_1/\delta_2)^{\mu} B_{n_2}. \tag{43}$$

Substituting this into eqn (41) yields

$$B_{n_3} = (\sigma_1 - \sigma_2)(\delta_3/\delta_2)^{\mu} B_{n_2}. \tag{44}$$

Thus, by using eqns (43) and (44), eqn (42) reduces to

$$(\sigma_1 - 1)\delta_1^{\mu} A_{n_1} + (\sigma_2 - 1)\delta_2^{\mu} A_{n_2} + \cot\mu\pi(-(\sigma_1 - 1)\delta_1^{2\mu} \\ + (\sigma_2 - 1)\delta_2^{2\mu} - (\sigma_1 - \sigma_2)\delta_3^{2\mu})\delta_2^{\mu} B_{n_2} - \delta_3^{\mu} A_{n_3} = 0. \tag{45}$$

Subcase II(b) : $1 < \mu < 2$. In this range, all terms in eqn (40) vanish as r approaches zero, except those containing $r^{-\mu+2j+1}$ for $j = 0$ and $r^{-\mu+2j-1}$ for $j = 0$ and $j = 1$. In the limit, the coefficients of $r^{-\mu-1}$ yield eqn (41), while the coefficients of $r^{-\mu+1}$ result in

$$(\sigma_1 - 1)(\delta_1/2)^{-\mu+2} B_{n_1} + (\sigma_2 - 1)(\delta_2/2)^{-\mu+2} B_{n_2} + (\delta_3/2)^{-\mu+1} B_{n_3} = 0. \tag{46}$$

Equations (38), (41) and (46) resolve to $B_{n_1} = B_{n_2} = B_{n_3} = 0$, because these equations are linearly independent homogeneous ones in B_{n_1}, B_{n_2} and B_{n_3}. Similarly, it can be shown that enforcing the rotation regularity condition [eqn (15c)] leads to the same relations obtained from satisfying eqn (15b); that is, eqn (45) in Subcase II(a) and $B_{n_1} = B_{n_2} = B_{n_3} = 0$ in Subcase II(b).

In the same manner, it is easy to show that $\mu > 2$ or integer values of μ result in $B_{n_1} = B_{n_2} = B_{n_3} = 0$.

FREQUENCY DETERMINANTS

In the development above, the general solution to the differential equations of motion [eqns (10)] and the associated simply supported radial edge boundary conditions [eqns (13)] are defined by eqns (12), with the radial variation being given by eqns (16) for $\lambda^4 < 1/RS$ and by eqns (36) for $\lambda^4 > 1/RS$. By invoking the regularity conditions at $r = 0$ [eqns (15)], three constraint relations among the integration constants A_{n_i} and B_{n_i} $(i = 1, 2, 3)$ have been derived, which are eqns (31)–(33) (for $0 < \mu < 1$ and $\lambda^4 < 1/RS$), eqns (43)–(45) (for $0 < \mu < 1$ and $\lambda^4 > 1/RS$), and the result $B_{n_1} = B_{n_2} = B_{n_3} = 0$ (for $\mu > 1$). Three additional equations are obtained by applying the boundary conditions along the circular

Table 1(a). Nondimensional frequency parameters $\omega a^2(\rho h/D)^{1/2}$ for sectorial plates having simply supported radial edges and clamped circular edge; mode shapes have no radial node lines ($\nu = 0.3$)

			$\omega a^2(\rho h/D)^{1/2}$			
α	μ	s	$h/a \cong 0$†	$h/a = 0.1$	$h/a = 0.2$	$h/a = 0.4$
		1	114.276	95.5089	68.0625	41.2164
		2	206.210	152.770	102.617	58.6756
30°	6.0	3	316.128	213.160	135.723	67.8976
		4	445.210	274.896	167.962	75.1689
		5	593.897	337.090	194.324	80.1025
		1	51.1225	45.8329	36.8449	24.2064
		2	111.092	91.5849	66.5856	40.1956
60°	3.0	3	190.440	143.520	97.2196	53.1441
		4	289.340	199.374	128.142	56.4001
		5	408.040	257.924	159.012	60.3729
		1	34.9281	32.2624	27.0400	18.5761
		2	84.6400	72.2500	54.6121	33.7561
90°	2.0	3	154.008	120.560	83.9056	47.8864
		4	242.736	174.240	114.276	50.2681
		5	351.563	231.040	144.962	54.1696
		1	27.7729	26.0100	22.3729	15.7609
		2	72.4201	63.0436	48.4416	30.5809
120°	1.5	3	136.656	109.203	77.2641	45.0241
		4	320.020	161.544	107.330	47.3344
		5	324.360	217.563	137.828	51.4089
		1	22.4676	21.2521	18.5761	13.5424
		2	62.8849	55.5025	[illegible]5600	27.8784
165°	1.0909	3	123.2100	100.0000	71.7409	42.5104
		4	203.063	151.044	101.606	45.0241
		5	302.760	206.497	131.790	49.2804
		1	21.3444	20.2500	17.8084	13.0321
		2	60.8400	53.8756	42.3801	27.2484
180°	1.0	3	120.122	98.0100	70.5600	41.9904
		4	199.092	148.840	100.200	44.6224
		5	297.908	203.918	130.645	48.8601

† Classical thin plate theory (Huang *et al.*, 1992).

edge ($r = a$). As a result, six homogeneous, algebraic equations in A_{n_i} and B_{n_i} are obtained from which the vanishing determinant of the sixth order coefficient matrix yields the eigenvalues

$$\bar{\lambda} = a\lambda = [\omega a^2(\rho h/D)^{1/2}]^{1/2}. \tag{47}$$

Three types of boundary conditions are considered along the circular edge

$$\text{clamped:} \quad W(a,\theta) = \psi_r(a,\theta) = \psi_\theta(a,\theta) = 0 \tag{48a}$$

$$\text{simply supported:} \quad W(a,\theta) = M_r(a,\theta) = \psi_\theta(a,\theta) = 0 \tag{48b}$$

$$\text{free:} \quad M_r(a,\theta) = M_{r\theta}(a,\theta) = Q_r(a,\theta) = 0. \tag{48c}$$

The sixth order frequency determinants resulting from each of the boundary conditions [eqns (57)] are easily reduced to fourth order by using eqns (31)–(33) or eqns (43)–(45). Elements of these fourth order determinants are presented in Appendix B.

NUMERICAL RESULTS

Shown in Tables 1–3 are accurate nondimensional frequencies $\omega a^2(\rho h/D)^{1/2}$ obtained for thick sectorial plates having simply supported radial edges, and clamped, simply supported, or free conditions along the circular edge. All frequencies tabulated correspond to mode shapes having no radial node lines. Tables 1–3 list the first five (nonzero) values

Table 1(b). Nondimensional frequency parameters $\omega a^2(\rho h/D)^{1/2}$ for sectorial plates having simply supported radial edges and clamped circular edge; mode shapes have no radial node lines ($\nu = 0.3$)

α	μ	s	$\omega a^2(\rho h/D)^{1/2}$ $h/a \cong 0$†	$h/a = 0.1$	$h/a = 0.2$	$h/a = 0.4$
		1	21.4829	19.6538	17.3163	12.6988
		2	60.9960	52.8999	14.6740	26.7598
195°	0.9231	3	120.242	96.6317	69.6263	41.5322
		4	199.213	147.215	99.1851	44.5697
		5	297.917	202.167	129.450	48.8592
		1	21.6581	19.3072	16.9829	12.4614
		2	61.1285	52.1801	41.0925	26.3704
210°	0.8571	3	120.371	95.6364	68.9117	41.1754
		4	199.339	146.009	98.3763	44.6322
		5	298.042	200.800	128.582	48.9224
		1	22.0881	18.7907	16.2102	11.7850
		2	61.4550	50.5139	39.4485	25.1970
270°	0.6667	3	120.690	93.0316	66.7843	39.9443
		4	199.651	142.641	95.9219	44.7984
		5	298.349	196.836	125.931	49.3737
		1	22.3038	18.7246	15.7963	11.3248
		2	61.6196	49.6543	38.3595	24.4074
330°	0.5455	3	120.851	91.4357	65.3261	39.0824
		4	199.808	140.429	94.2448	44.8374
		5	298.505	194.153	124.142	49.8352
		1	22.3733	18.7212	15.6372	11.1376
		2	61.6729	49.3365	37.9250	24.1020
360°	0.5000	3	120.903	90.8082	64.7472	38.7503
		4	199.860	139.546	93.5896	44.8399
		5	298.555	193.079	123.454	50.0273
		1	10.216	9.941‡	9.240‡	7.468
		2	39.771	36.479‡	30.211‡	20.422
Complete circular		3	89.104	75.664‡	56.682‡	34.946
		4	158.183	123.319‡	85.571‡	49.675
		5	247.005	176.415	115.555	54.298

† Classical thin plate theory (Huang *et al.*, 1992).
‡ Irie *et al.* (1980).

satisfying the vanishing frequency determinants, $\det[C_{ij}] = 0$, defined in Appendix B. Results are shown for various salient angles ($\alpha \leqslant 180°$) (Tables 1a, 2a, 3a) and re-entrant corner angles ($\alpha > 180°$) (Tables 1b, 2b, 3b) and thickness ratios ($h/a = 0.1$, 0.2 and 0.4). A Poisson's ratio of $\nu = 0.3$ has been used to calculate $\omega a^2(\rho h/D)^{1/2}$ for the simply supported and free circular edge plates, but not the clamped circular edge ones, because in the latter $\det[C_{ij}] = 0$ and $\omega a^2(\rho h/D)^{1/2}$ is independent of ν (see Appendix B). Double precision (14 significant digit) arithmetic on an IBM 3090 machine has been used in evaluating the vanishing frequency determinants.

For the thin sectorial plate results shown in Tables 1–3 (i.e. $h/a \cong 0$), the number of nodal circles appearing in the mode shapes is $s-1$. For the thick sectorial plates, the mode number (s) indicates the order of the frequencies without consistently representing the number of nodal circles. That is, it is possible for modes which exhibit predominantly thickness-shear actions to appear among the first five frequencies in the thickest case ($h/a = 0.4$).

The focus of discussion here is to explore for the first time the variation of thick sectorial plate frequencies, as the sector angle (α) and thickness ratio (h/a) increase. For constant α, the frequency parameters, $\omega a^2(\rho h/D)^{1/2}$, shown in Tables 1–3 decrease as h/a increases, due to the inherent shear deformation and rotary inertia present. It should be noted, however, that as h/a increases, an alternative form of the frequency parameter, $\omega a(\rho/E)^{1/2}$, increases in the lower modes, while in some of the higher ones this parameter decreases. The latter situation occurs when the thickness-shear modes appear among the frequencies shown.

Table 2(a). Nondimensional frequency parameters $\omega a^2(\rho h/D)^{1/2}$ for sectorial plates having all edges simply supported; mode shapes have no radial node lines ($\nu = 0.3$)

α	μ	s	$\omega a^2(\rho h/D)^{1/2}$ $h/a \cong 0$†	$h/a = 0.1$	$h/a = 0.2$	$h/a = 0.4$
		1	98.0100	84.4561	64.8025	40.7044
		2	184.145	144.000	100.601	53.8756
30°	6.0	3	288.660	205.636	134.560	58.8289
		4	412.496	268.304	167.444	72.2500
		5	556.0164	331.968	176.358	75.3424
		1	40.0689	37.4544	32.1489	22.9441
		2	94.6729	81.9025	63.0436	44.3556
60°	3.0	3	168.740	134.096	94.8686	44.3561
		4	262.764	190.992	126.788	55.9504
		5	376.360	250.906	158.508	57.4564
		1	25.7049	24.5025	21.9961	16.8100
		2	70.2244	62.7264	50.4100	33.1776
90°	2.0	3	134.328	110.881	81.1801	42.2500
		4	218.448	165.123	112.572	49.1401
		5	321.844	223.503	144.240	52.8529
		1	19.4481	18.8356	17.2225	13.6900
		2	58.9824	53.5824	43.9569	29.7025
120°	1.5	3	118.374	99.4009	74.1321	41.3449
		4	197.403	152.276	105.473	45.5625
		5	295.840	209.670	136.890	50.6944
		1	14.8996	14.5161	13.5424	11.1556
		2	50.4100	46.3761	38.8129	26.8324
165°	1.0909	3	105.678	90.2500	68.3929	40.8321
		4	180.634	141.848	99.4009	42.6409
		5	275.228	198.246	130.645	49.0000
		1	13.9129	13.6161	12.7449	10.5625
		2	48.5809	44.7561	37.6996	26.1121
180°	1.0	3	102.8196	88.1721	67.0761	40.7044
		4	176.890	139.476	98.0100	41.9904
		5	270.603	195.720	129.277	48.7204

† Classical thin plate theory (Huang et al., 1992).

Considering now the frequency changes with increasing sector angle, one observes in Tables 1(a), 2(a) and 3(a) for the salient angles ($\alpha \leqslant 180°$) that $\omega a^2(\rho h/D)^{1/2}$ decreases markedly for all modes. This is expected, since the circumferential distance between radial supports increases with increasing α, which in turn decreases the stiffness of the plate. Conversely, as $\alpha \Rightarrow 0$, $\omega a^2(\rho h/D)^{1/2}$ becomes infinite for all modes.

However, frequency changes with increasing α are more interesting for the re-entrant sector angles. For h/a = constant, the frequency parameters, $\omega a^2(\rho h/D)^{1/2}$, are seen in Tables 1(b), 2(b) and 3(b) to change minimally over the range $195° \leqslant \alpha \leqslant 360°$, with the most rapid changes occurring for the smaller α within this range. Frequency results are shown for $\alpha = 330°$ to ascertain that no drastic changes in $\omega a^2(\rho h/D)^{1/2}$ occur due to the "notch effect" as $\alpha \Rightarrow 360°$. For the clamped, simply supported, and free circular edge plates, one can see that the frequency parameters obtained by using classical thin plate theory increase as α increases. In contrast, the frequency parameters obtained for the thick, clamped and simply supported circular edge plates [Tables 1(b) and 2(b)] decrease as α increases, except in the fourth and fifth modes of sectorial plates having $h/a = 0.4$. For the free circular edge thick plates [Table 3(b)], $\omega a^2(\rho h/D)^{1/2}$ decreases as α increases, except in the lowest frequency mode, which shows an increase as α increases. This is because the lowest frequency of a semicircular plate ($\alpha = 180°$) is zero, which corresponds to a rigid body rotation of the plate about its hinged diameter.

The case of the sectorial plate having a free circular edge is interesting for re-entrant corners, particularly for α in the vicinity of 180°. Consider the fundamental (i.e. lowest) frequency when $\alpha = 195°$. Table 3(b) shows a drastic difference in $\omega a^2(\rho h/D)^{1/2}$ between the value 1.4045 obtained from classical, thin plate theory and that (0.6437) for $h/a = 0.1$ obtained from the present analysis using Mindlin theory. With increasing α, the percentage

Table 2(b). Nondimensional frequency parameters $\omega a^2(\rho h/D)^{1/2}$ for sectorial plates having all edges simply supported; mode shapes have no radial node lines ($\nu = 0.3$)

			$\omega a^2(\rho h/D)^{1/2}$			
α	μ	s	$h/a \cong 0$†	$h/a = 0.1$	$h/a = 0.2$	$h/a = 0.4$
195°	0.9231	1	14.0366	13.0907	12.2635	10.1789
		2	48.6272	43.8256	36.8698	25.6359
		3	102.921	86.7871	66.1120	40.6992
		4	176.949	137.815	96.9459	41.5570
		5	270.714	193.857	128.194	48.8114
210°	0.8571	1	14.1458	12.7827	11.9323	9.8862
		2	48.7447	43.1490	36.2766	25.2323
		3	103.038	85.8045	65.3660	40.5343
		4	177.066	136.600	96.1105	41.4591
		5	270.831	192.466	127.299	48.9203
270°	0.6667	1	14.4129	12.3598	11.2021	9.0707
		2	49.0344	41.6562	34.6347	24.0044
		3	103.328	83.2835	63.1562	39.3606
		4	177.356	133.239	93.5760	41.9031
		5	271.121	188.457	124.570	48.6619
330°	0.5455	1	14.5467	12.3463	10.8524	8.5444
		2	49.1807	40.9486	33.5701	23.1641
		3	103.474	81.7788	61.6466	38.4878
		4	177.503	131.054	91.8415	42.3444
		5	271.268	185.753	122.730	48.1372
360°	0.5000	1	14.5897	12.3639	10.7267	8.3378
		2	49.2279	40.6969	33.1474	22.8353
		3	103.522	81.1927	61.0470	38.1517
		4	177.550	130.183	91.1627	42.5261
		5	271.315	184.672	122.022	47.9014
Complete circular		1	4.9352	4.894	4.777	4.396
		2	29.7200	28.240	24.994	18.658
		3	74.156	65.942	52.514	34.287
		4	138.318	113.574	82.766	45.177
		5	222.215	167.530	113.875	49.886

† Classical thin plate theory (Huang *et al.*, 1992).

difference in fundamental frequencies obtained from these two plate theories becomes less. Moreover, the drastic difference occurs only for the fundamental mode, where the large inertial moment about the diametral axis ($\theta = \pm 90°$) of the vibrating plate must be principally equilibrated by shearing forces distributed along the simply supported radial edges. [The twisting moment ($M_{r\theta}$) along the simple supports is expected to be small.] The shearing force, however, will be large, because of the small moment arm available, $r \sin(\alpha/2)$. The large shearing force becomes significant in the Mindlin theory, where shear deformation effects are included. Nonetheless, in the higher modes additional circumferential node lines exist, which are equivalent to knife edge supports. These equivalent knife edge supports, along with the radial edge simple supports, are equilibrated by considerably smaller inertial moments in the higher modes. Similarly, for the other circular edge conditions (i.e. clamped and simply supported, Tables 1 and 2), there appears to be no difficulty in the convergence of the fundamental frequencies for $h/a = 0.1$ to the classical theory ($h/a \cong 0$), since the circular edges transmit shear forces that aid in maintaining the dynamic moment equilibrium of the plates.

Another reason for the large differences in fundamental frequency predicted by the thick and thin plate theories lies in the differences in shear stress singularities at the re-entrant corner. As discussed in Appendix C, according to Mindlin theory, the shear force varies as $r^{\mu-1}$ in the vicinity of $r = 0$ for $0 < \mu < 1$ ($\alpha > 180°$) and no such singularities occur for $\mu \geqslant 1$ ($\alpha \geqslant 180°$). These findings, which are quite different from those surmised by using classical thin plate theory (Leissa *et al.*, 1992), are supported by the data shown in Tables 4 and 5. Listed therein are nondimensional frequencies for nearly semicircular plates ($\alpha = 178°$, 179°, 181° and 182°) with simply supported radial edges and free circular

Table 3(a). Nondimensional frequency parameters $\omega a^2(\rho h/D)^{1/2}$ for sectorial plates having simply supported radial edges and free circular edge; mode shapes have no radial node lines ($\nu = 0.3$)

α	μ	s	$\omega a^2(\rho h/D)^{1/2}$			
			$h/a \cong 0$†	$h/a = 0.1$	$h/a = 0.2$	$h/a = 0.4$
		1	47.4721	43.2556	36.3525	25.4611
		2	128.766	101.481	74.9835	49.4448
30°	6.0	3	291.499	160.362	108.985	66.8339
		4	320.410	221.724	140.807	76.2373
		5	448.592	284.405	183.326	83.1343
		1	12.4609	12.0645	11.3138	9.4827
		2	53.1441	48.2275	39.9601	26.9454
60°	3.0	3	112.148	94.5309	70.8627	47.4666
		4	190.716	147.992	102.271	53.0625
		5	289.340	205.725	132.874	63.5496
		1	5.3824	5.2781	5.1144	4.6406
		2	35.2836	33.0338	28.6685	20.6416
90°	2.0	3	84.4561	73.8757	57.7235	35.5860
		4	153.512	123.772	88.5312	46.5424
		5	242.114	179.260	119.308	56.6482
		1	2.6896	2.6651	2.6195	2.4746
		2	27.5625	26.1080	23.2208	17.3914
120°	1.5	3	76.7401	63.9168	51.0925	32.5870
		4	135.956	111.797	81.4903	44.0020
		5	219.632	166.008	112.256	53.1281
		1	0.7921	0.7869	0.7813	0.7614
		2	21.7756	20.8319	18.9129	14.6919
165°	1.0909	3	61.9369	55.9893	45.6462	29.9767
		4	122.103	102.083	75.643	42.4517
		5	201.924	155.162	106.360	50.2766
		1	0.0‡	0.0‡	0.0‡	0.0‡
		2	20.5209	19.7109	17.9784	14.0888
180°	1.0	3	59.9076	54.2580	44.4342	29.3764
		4	119.0286	99.9360	74.3320	42.1967
		5	197.765	152.752	105.034	49.6602

† Classical thin plate theory (Huang et al., 1992).
‡ Rigid body rotation.

edge and thickness ratios ranging from classically thin ($h/a \cong 0$) to very thick ($h/a = 0.4$). Indeed, as h/a increases in the range $0.02 \leqslant h/a \leqslant 0.4$, $\omega a^2(\rho h/D)^{1/2}$ decrease albeit minimally.

Theoretically speaking, the influence of shear forces is reflected in the potential energy of the Mindlin theory, whereas such forces are inherently absent from the potential energy derived from the classical plate theory. In Mindlin theory, the singularities of shear forces contribute a significant amount of energy such that the fundamental frequencies of nearly semicircular plates with $\alpha = 181°$ and $182°$ with $h/a = 0.02$ (Table 4) are substantially reduced from those obtained for the classically thin plates ($h/a \cong 0$) by approximately 66.5% and 65.2%, respectively. In contrast, no shear singularities exists for $\alpha \leqslant 180°$, although a small influence of transverse shears is evidenced by the fundamental frequencies for $\alpha = 178°$ and $\alpha = 179°$ with $h/a = 0.02$ (Table 4), which are reduced from those frequencies for $h/a \cong 0$ by approximately 2.3% and 3.7%, respectively.

Unfortunately, computational difficulties prevented extending the frequencies results of Tables 4 and 5 to $h/a < 0.02$. As $h/a \Rightarrow 0$, the arguments ($\bar{\delta}_i$) become prohibitively large for proper numerical evaluation of the modified Bessel functions of the second kind (Y_μ and K_μ in the frequency determinants (Appendix B).

The results of Table 3(b) are extended to thinner plates in Table 6, where frequencies are given for $195° \leqslant \alpha \leqslant 360°$ and for $h/a = 0.02$, 0.03 and 0.05. It is interesting to note the significant difference in $\omega a^2(\rho h/D)^{1/2}$ calculated using the thick (Mindlin) and thin (classical) plate theories, even for the small thickness ratio of $h/a = 0.02$. The difference in $\omega a^2(\rho h/D)^{1/2}$ is more pronounced for $\alpha \Rightarrow 180°$ and less for $\alpha \Rightarrow 360°$. Clearly, one can see in Table 4 that the shear singularities derived from Mindlin theory contribute significantly in reducing the potential energy of thin sectorial plates having re-entrant angles α.

Table 3(b). Nondimensional frequency parameters $\omega a^2(\rho h/D)^{1/2}$ for sectorial plates having simply supported radial edges and free circular edge; mode shapes have no radial node lines ($\nu = 0.3$)

α	μ	s	$\omega a^2(\rho h/D)^{1/2}$ $h/a \cong 0$†	$h/a = 0.1$	$h/a = 0.2$	$h/a = 0.4$
		1	1.4045	0.6437	0.5974	0.5422
		2	20.5428	19.0860	17.4162	13.6673
195°	0.9231	3	59.9349	53.2445	43.6628	28.9816
		4	119.084	98.6168	73.4343	40.5994
		5	198.003	151.212	104.085	42.3157
		1	1.8884	1.0422	0.9414	0.8253
		2	20.5959	18.6476	16.9773	13.3101
210°	0.8571	3	60.0327	52.4741	43.0216	28.6269
		4	119.185	97.5610	72.6619	40.3919
		5	198.107	149.942	103.254	42.1498
		1	2.7586	2.0614	1.8052	1.4960
		2	20.7233	17.8576	15.8946	12.2763
270°	0.6667	3	60.2745	50.6900	41.2080	27.5015
		4	119.434	94.7908	70.3547	39.8251
		5	198.364	146.388	100.719	41.5890
		1	3.1164	2.5769	2.2498	1.8188
		2	20.7858	17.6299	15.2906	11.5953
330°	0.5455	3	60.3959	49.7738	40.0081	26.6996
		4	119.560	93.0921	68.7747	39.4656
		5	198.495	144.052	98.9829	41.1970
		1	3.2248	2.7389	2.3916	1.9158
		2	20.8057	17.5718	15.0640	11.3300
360°	0.5000	3	60.4364	49.4371	39.5301	26.3809
		4	119.600	92.4253	68.1493	39.3228
		5	198.537	143.119	98.3051	41.0526
		1	0.0‡	0.0‡	0.0‡	0.0‡
		2	9.003	8.868§	8.505§	7.464
Complete circular		3	38.443	36.041§	31.111§	22.268
		4	87.750	76.676§	59.645§	36.935
		5	156.82	126.274§	90.059§	47.418

† Classical thin plate theory (Huang *et al.*, 1992).
‡ Rigid body rotation.
§ Irie *et al.* (1980).

As α approaches 360°, the radial boundaries of the sectorial plate become coincident, forming a hinged crack with no circumferential moment (M_θ) transferred across the boundaries. The frequencies of these plates may be compared with the corresponding ones (i.e. no radial node lines) for complete circular plates (Tables 1–3). The frequencies of the complete circular plates are lower than those of the 360° sectorial plates, since the stiffnesses of the latter are typically larger due to the presence of the hinged crack.

CONCLUDING REMARKS

The first known exact analytical solutions have been derived here for the flexural vibrations of thick (Mindlin) sectorial plates having simply supported radial edges. The general solution involves non-integer order ordinary and modified Bessel functions of the first and second kinds, and six constants of integration. The analytical procedure requires one to enforce the nine boundary conditions along the radial and circular edges, and the three regularity conditions at the vertex of the radial edges.

Frequency determinant equations have been derived for Mindlin sectorial plates having clamped, simply supported, or free circular boundaries. Nondimensional frequency parameters have been calculated for each of these plate configurations for both salient ($\alpha \leqslant 180°$) and re-entrant ($\alpha > 180°$) sector angles, and a variety of thickness ratios (h/a).

In certain special cases, solutions for sectorial plates having simply supported radial edges may be adapted from the solutions for complete circular plates with clamped, simply supported, or free boundaries. This is possible when the sector angle (α) is an integer

Table 4. Nondimensional frequencies for nearly semicircular thick plates having simply supported radial edges and free circular edge; ($\nu = 0.3$)

α	μ	s	$\omega a^2(\rho h/D)^{1/2}$ $h/a \cong 0$†	$h/a = 0.1$	$h/a = 0.2$	$h/a = 0.4$
		1	0.2601	0.2537	0.2524	0.2473
		2	20.7025	19.8488	18.0931	14.1632
178°	1.0112	3	60.2176	54.4718	44.5837	29.4512
		4	119.465	100.202	74.4942	42.2253
		5	198.528	153.049	105.198	49.7363
		1	0.1849	0.1777	0.1768	0.1734
		2	20.6116	19.7794	18.0353	14.1256
179°	1.0056	3	60.0625	54.3641	44.5089	29.4133
		4	119.246	100.068	74.4131	42.2110
		5	198.246	152.898	105.116	49.6983
		1	0.0‡	0.0‡	0.0‡	0.0‡
		2	20.5209	19.7109	17.9784	14.0888
180°	1.0	3	59.9076	54.2580	44.4342	29.3764
		4	119.029	99.9360	74.3320	42.1967
		5	197.765	152.752	105.034	49.6602
		1	0.3844	0.1262	0.1246	0.1212
		2	20.5209	19.6621	17.9361	14.0580
181°	0.9945	3	59.9076	54.1814	44.3782	29.3482
		4	119.028	99.8381	74.2682	40.2399
		5	197.965	152.6386	104.9662	40.8334
		1	0.5476	0.1839	0.1801	0.1739
		2	20.5209	19.6152	17.8946	14.0280
182°	0.9890	3	59.9076	54.1049	44.3223	29.3211
		4	119.028	99.7422	74.2044	40.2399
		5	197.965	152.527	104.901	40.8155

† Classical thin plate theory (Huang *et al.*, 1992).
‡ Rigid body rotation.

Table 5. Nondimensional frequencies for nearly semicircular thick plates having simply supported radial edges and free circular edge ($\nu = 0.3$)

α	μ	s	$\omega a^2(\rho h/D)^{1/2}$ $h/a \cong 0$†	$h/a = 0.02$	$h/a = 0.03$	$h/a = 0.05$
		1	0.2601	0.2541	0.2541	0.2540
		2	20.7025	20.5816	20.5372	20.4060
178°	1.0112	3	60.2176	59.7931	59.4641	58.4598
		4	119.465	118.2771	117.023	113.318
		5	198.528	195.5020	192.150	182.680
		1	0.1849	0.1781	0.1780	0.1780
		2	20.6116	20.5064	20.4630	20.3329
179°	1.0056	3	60.0625	59.6648	59.3362	58.3375
		4	119.246	118.096	116.845	113.150
		5	198.246	—	—	182.474
		1	0.0‡	0.0‡	0.0‡	0.0‡
		2	20.5209	20.4331	20.3897	20.2608
180°	1.0	3	59.9076	59.5382	59.2115	58.2154
		4	119.029	117.916	116.668	112.984
		5	197.765	195.035	191.701	182.272
		1	0.3844	0.1288	0.1282	0.1274
		2	20.5209	20.3816	20.3383	20.2095
181°	0.9945	3	59.9076	59.4472	59.1223	58.1284
		4	119.028	117.788	116.543	112.865
		5	197.965	—	191.540	182.123
		1	0.5476	0.1907	0.1891	0.1870
		2	20.5209	20.3311	20.2878	20.1592
182°	0.9890	3	59.9076	59.3609	59.0346	58.0446
		4	119.028	117.662	116.420	112.748
		5	197.965	194.709	191.382	181.977

† Classical thin plate theory (Huang *et al.*, 1992).
‡ Rigid body rotation.

Table 6. Nondimensional frequency parameters $\omega a^2(\rho h/D)^{1/2}$ for thin sectorial plates having simply supported radial edges and free circular edge; mode shapes have no radial node lines ($\nu = 0.3$)

α	μ	s	$\omega a^2(\rho h/D)^{1/2}$			
			$h/a \cong 0$†	$h/a = 0.02$	$h/a = 0.03$	$h/a = 0.05$
		1	1.4045	0.7569	0.7172	0.6867
		2	20.5428	19.8916	19.7723	19.6311
195°	0.9231	3	59.9349	58.5225	58.1132	57.1170
		4	119.084	116.4241	115.077	111.435
		5	198.003	193.2100	189.635	180.322
		1	1.8884	1.2544	1.1997	1.1449
		2	20.5959	19.5364	19.4313	19.2721
210°	0.8571	3	60.0327	57.9121	57.4321	56.4001
		4	119.185	115.563	114.015	110.460
		5	198.107	191.823	188.189	179.024
		1	2.7586	2.4649	2.3855	2.2801
		2	20.7233	19.6249	19.3134	18.9225
270°	0.6667	3	60.2745	57.6081	56.7581	55.2049
		4	119.434	114.490	112.460	108.160
		5	198.364	189.888	185.633	175.563
		1	3.1164	2.9929	2.9080	2.8224
		2	20.7858	19.9809	19.5974	19.0096
330°	0.5455	3	60.3959	58.0644	56.9965	55.0564
		4	119.560	114.918	112.335	107.330
		5	198.495	189.888	—	173.976
		1	3.2248	3.1329	3.0594	2.9929
		2	20.8057	20.0704	19.7154	19.0969
360°	0.5000	3	60.4364	58.3696	57.1385	55.0564
		4	119.600	115.133	112.375	106.916
		5	198.537	190.164	184.808	173.449

† Classical thin plate theory (Huang *et al.*, 1992).

submultiple of 180° (i.e. $\alpha = 180/n$, $n = 1, 2, 3, \ldots$). The frequencies and mode shapes of these sectorial plates are identical to the complete circular ones having nodal diameters, because the nodal diameters of the latter duplicate the simply supported radial edges of the sectorial plates.

Frequency results obtained for Mindlin sectorial plates have been compared to those determined previously for classically thin sectorial plates. It was found that the shear deformation effects are especially important for the fundamental frequencies of plates having sector angles slightly in excess of 180° when the circular boundary is free, due to the large shear forces developed at the radial edges. Basically, the shear forces near $r = 0$ of thick sectorial plates varies as $r^{\mu-1}$ for $0 < \mu < 1$ ($\alpha > 180°$). For $\mu \geqslant 1$ ($\alpha \leqslant 180°$), no singular shear forces exist at the vertex of thick sectorial plates. These singular shear forces contribute significantly to the potential energy of thick (Mindlin) sectorial plates. Besides this, the frequencies for 360° sectorial plates (i.e. circular plates stiffened by a hinged crack) have been compared with those for complete circular ones.

Acknowledgement—This research was supported by the National Science Foundation, Award No. MSS-9157972.

REFERENCES

Ben-Amoz, M. (1959). Note on deflections and flexural vibrations of clamped sectorial plates. *ASME J. appl. Mech.* **26**, 136–137.
Bhattacharya, A. P. and Bhowmic, K. N. (1975). Free vibration of a sectorial plate. *J. Sound Vibr.* **41**, 503–505.
Bapu Rao, M. N., Guruswamy, P. and Sampath Kumaran, K. S. (1977). Finite element analysis of thick annular and sector plates. *Int. J. Nuclear Engng Design* **41**, 247–255.
Callahan, W. R. (1955). On the flexural vibrations of circular and elliptic plates. *Quart. appl. Math.* **13**, 371–380.
Cheung, M. S. and Chan, M. Y. T. (1981). Static and dynamic analysis of thin and thick sectorial plates by finite strip method. *Comput. Struct.* **14**, 79–88.
Guruswamy, P. and Yang, T. Y. (1979). A sector finite element for dynamic analysis of thick plates. *J. Sound Vibr.* **62**, 505–516.
Huang, C. S., Leissa, A. W. and McGee, O. G. (1993). Exact analytical solutions for the vibrations of sectorial plates with simply supported radial edges. *ASME J. appl. Mech.* **60**, 478–483.

Irie, T., Yamada, G. and Aomura, S. (1979). Free vibration of a Mindlin annular plate of varying thickness. *J. Sound Vibr.* **66,** 187–197.

Irie, T., Yamada, G. and Aomura, S. (1980). Natural frequencies of Mindlin circular plates. *ASME J. appl. Mech.* **47,** 652–655.

Irie, T., Yamada, G. and Takagi, K. (1982). Natural frequencies of thick annular plates. *ASME J. appl. Mech.* **49,** 633–638.

Leissa, A. W. (1969). Vibration of plates. NASA SP-160, U.S. Government Printing Office.

Leissa, A. W. (1977). Recent research in plate vibrations (1973–1976): complicating effects. *Shock Vibr. Digest* **10,** 21–35.

Leissa, A. W. (1981). Plate vibration research (1976–1980): complicating effects. *Shock and Vibr. Digest* **13,** 19–36.

Leissa, A. W. (1987). Recent studies in plate vibration (1981–1985): part II, complicating effects. *Shock Vibr. Digest* **19,** 10–24.

Leissa, A. W., McGee, O. G. and Huang, C. S. (1993). Vibrations of sectorial plates having corner stress singularities. *ASME J. appl. Mech.* **60,** 134–140.

Maruyama, K. and Ichinomiya, O. (1981). Experimental investigation of free vibrations of clamped sector plates. *J. Sound Vibr.* **74,** 563–573.

Mindlin, R. D. and Deresiewicz, H. (1954). Thickness-shear and flexural vibrations of a circular disk. *J. appl. Phys.* **25,** 1329–1332.

Rao, S. S. and Prasad, A. S. (1975). Vibrations of annular plates including the effects of rotary inertia and transverse shear deformation. *J. Sound Vibr.* **42,** 305–324.

Rubin, C. (1975). Nodal circles and natural frequencies for the isotropic wedge. *J. Sound Vibr.* **39,** 523–526.

Srinivasan, R. S. and Thiruvenkatachari, V. (1985). Free vibration of transverse isotropic annular sector Mindlin plates. *J. Sound Vibr.* **101,** 193–201.

Tranter, C. J. (1968). *Bessel Functions with Some Physical Applications.* English University Press.

Westmann, R. A. (1962). A note on free vibrations of triangular and sector plates. *J. Aerospace Sci.* **29,** 1139–1140.

Williams, M. L. (1952). Surface stress signularities resulting from various boundary conditions in angular plates under bending. *Proceedings of the First U.S. National Congress of Applied Mechanics*, pp. 325–329.

APPENDIX A: INVESTIGATION OF THE SECOND REGULARITY CONDITION FOR EDGE ROTATION

Using eqns (6a), (12) and (16), the second rotation regularity condition given by eqn (15c) results in

$$\lim_{r\to 0}[(\sigma_1-1)(\mu/r)[A_{n_1}J_\mu(\delta_1 r)+B_{n_1}Y_\mu(\delta_1 r)]+(\sigma_2-1)(\mu/r)[A_{n_2}I_\mu(\delta_2 r)+B_{n_2}K_\mu(\delta_2 r)]$$
$$-\delta_3[A_{n_3}I'_\mu(\delta_3 r)+B_{n_3}K'_\mu(\delta_3 r)]] = \text{finite.} \quad \text{(A1)}$$

Applying eqns (17), (19), (21) and (24) to eqn (A1) yields

$$\begin{aligned}\lim_{r\to 0}\sum_{j=0,1}^{\infty} & [(\sigma_1-1)(\mu/r)(A_{n_1}(-1)^j(\delta_1 r/2)^{\mu+2j}\cdot[j!\Gamma(\mu+j+1)]^{-1}\\
&+B_{n_1}(\cot\mu\pi\cdot[(-1)^j(\delta_1 r/2)^{\mu+2j}]\cdot[j!\Gamma(\mu+j+1)]^{-1}\\
&-[\sin\mu\pi]^{-1}\cdot[(-1)^j(\delta_1 r/2)^{-\mu+2j}]\cdot[j!\Gamma(-\mu+j+1)]^{-1}))\\
&+(\sigma_2-1)(\mu/r)(A_{n_2}(\delta_2 r/2)^{\mu+2j}\cdot[j!\Gamma(\mu+j+1)]^{-1}\\
&+B_{n_2}(\pi/(2\sin\mu\pi)\cdot(\delta_2 r/2)^{-\mu+2j}\cdot[j!\Gamma(-\mu+j+1)]^{-1}\\
&-(\delta_2 r/2)^{\mu+2j}\cdot[j!\Gamma(-\mu+j+1)]^{-1}))-\delta_3(A_{n_3}(\delta_3 r/2)^{\mu+2j-1}\cdot[2j!\Gamma(\mu+j)]^{-1}\\
&-B_{n_3}(\pi/4)([\sin(\mu-1)\pi]^{-1}((\delta_3 r/2)^{-\mu+2j+1}\cdot[j!\Gamma(-\mu+j+2)]^{-1}\\
&-(\delta_3 r/2)^{\mu+2j-1}\cdot[j!\Gamma(\mu+j)]^{-1})\\
&+[\sin(\mu+1)\pi]^{-1}(\delta_3 r/2)^{-\mu+2j-1}\cdot[j!\Gamma(-\mu+j)]^{-1}))] = \text{finite.}\end{aligned} \quad \text{(A2)}$$

*Case A*1: $0<\mu<1$

In this range, all terms in eqn (A2) vanish in the limit, except those for $j=0$. The remaining terms contain $r^{\mu-1}$ and $r^{-\mu-1}$. From the coefficients of $r^{-\mu-1}$

$$((\sigma_1-1)\mu(\delta_1/2)^{-\mu}[\Gamma(-\mu+1)\cdot\sin\mu\pi]^{-1})B_{n_1}-((\sigma_2-1)(\mu\pi/2)(\delta_2/2)^{-\mu}\cdot[\Gamma(-\mu+1)\cdot\sin\mu\pi]^{-1})B_{n_2}$$
$$-((\delta_3\pi/4)(\delta_3/2)^{-\mu}\cdot[\Gamma(-\mu)\cdot\sin(\mu+1)\pi]^{-1})B_{n_3}=0. \quad \text{(A3)}$$

Since $\sin(\mu+1)\pi=-\sin\mu\pi$ and $\Gamma(-\mu+1)=-\mu\Gamma(-\mu)$, eqn (A3) simplifies to

$$(\sigma_1-1)\delta_1^{-\mu}B_{n_1}-(\pi/2)(\sigma_2-1)\delta_2^{-\mu}B_{n_2}-(\pi/2)\delta_3^{-\mu}B_{n_3}=0. \quad \text{(A4)}$$

From the coefficients of $r^{\mu-1}$

$$((\sigma_1-1)\mu(\delta_1/2)^{\mu}[\Gamma(\mu+1)]^{-1})A_{n_1}+((\sigma_1-1)\cdot\mu\cot\mu\pi\cdot(\delta_1/2)^{\mu}[\Gamma(\mu+1)]^{-1})B_{n_1}$$
$$+((\sigma_2-1)\mu(\delta_2/2)^{\mu}[\Gamma(\mu+1)]^{-1})A_{n_2}-((\sigma_2-1)\cdot\mu\pi/(2\sin\mu\pi)\cdot(\delta_2/2)^{\mu}[\Gamma(\mu+1)]^{-1})B_{n_2}$$
$$-((\delta_3/2)^{\mu}[\Gamma(\mu)]^{-1})A_{n_3}-(\pi/(2\sin(\mu-1)\pi)\cdot(\delta_3/2)^{\mu}[\Gamma(\mu)]^{-1})B_{n_3}=0. \quad \text{(A5)}$$

Since $\sin(\mu-1)\pi = -\sin\mu\pi$ and $\Gamma(\mu+1) = \mu\Gamma(\mu)$, eqn (A5) reduces to

$$(\sigma_1-1)\delta_1^{\mu}A_{n_1}+(\sigma_1-1)\cdot\cot\mu\pi\cdot\delta_1^{\mu}B_{n_1}+(\sigma_2-1)\delta_2^{\mu}A_{n_2}$$
$$-(\sigma_2-1)\cdot\delta_2^{\mu}\cdot\pi/(2\sin\mu\pi)B_{n_2}-\delta_3^{\mu}A_{n_3}+\delta_3^{\mu}\cdot\pi/(2\sin\mu\pi)B_{n_3}=0. \quad \text{(A6)}$$

Equations (A4) and (A6) are identical to eqns (28) and (30), respectively.

Subcase I(b): $1 < \mu < 2$. In this range, all terms in eqn (A2) vanish as r approaches zero, except those terms containing $r^{-\mu+1+2j}$ for $j = 0$ and $r^{-\mu-1+2j}$ for $j = 0$ and $j = 1$. The remaining terms contain $r^{-\mu+1}$ and $r^{-\mu-1}$. In the limit the coefficients of $r^{-\mu-1}$ yield eqn (A4). From the coefficients of $r^{-\mu+1}$

$$(\sigma_1-1)\mu((\delta_1/2)^{-\mu+2}\cdot[\Gamma(-\mu+2)\cdot\sin\mu\pi]^{-1})B_{n_1}$$
$$+(\sigma_2-1)\cdot\mu\pi/2((\delta_2/2)^{-\mu+2}\cdot[\Gamma(-\mu+2)\cdot\sin\mu\pi]^{-1})B_{n_2}$$
$$+((\delta_3\pi/4)(\delta_3/2)^{-\mu+1}\cdot[\Gamma(-\mu+2)\cdot\sin(\mu-1)\pi]^{-1}$$
$$-(\delta_3/2)^{-\mu+1}\cdot[\Gamma(-\mu+1)\cdot\sin(\mu+1)\pi]^{-1})B_{n_3}=0. \quad \text{(A7)}$$

Using $\sin(\mu-1)\pi = -\sin\mu\pi$ and $\Gamma(-\mu+1) = (-\mu+1)\Gamma(-\mu+1)$, eqn (A7) simplifies to

$$(\sigma_1-1)\delta_1^{-\mu+2}B_{n_1}+(\sigma_2-1)(\pi/2)\delta_2^{-\mu+2}B_{n_2}-(\pi/2)\delta_3^{-\mu+2}B_{n_3}=0. \quad \text{(A8)}$$

The three linearly independent eqns (22), (A4) and (A8) result in $B_{n_1} = B_{n_2} = B_{n_3} = 0$.

APPENDIX B: ELEMENTS OF FREQUENCY DETERMINANTS

For simplicity of the calculations, the following nondimensional variables are introduced [see eqns (8) and (9)]

$$\bar{\delta}_i = a\delta_i, \quad \bar{R} = R/a^2, \quad \bar{S} = S/a^2. \quad \text{(B1)}$$

Elements of the vanishing fourth order frequency determinant, $\det[C_{ij}] = 0$, $(i, j = 1, 2, 3, 4)$ are given below for each of the circular edge conditions described by eqns (57). Different forms are required for $0 < \mu < 1$ ($\alpha > 180°$) and for $\mu > 1$ ($\alpha < 180°$). Besides this, the determinant forms depend upon whether $\bar{\lambda}^4 < 1/\bar{R}\bar{S}$ or $\bar{\lambda}^4 > 1/\bar{R}\bar{S}$.

When $0 < \mu < 1$, there are no radial node lines in the free vibration mode shapes. Mode shapes with radial node lines result from $\mu > 1$, because radial node lines duplicate simply supported boundary conditions.

For $0 < \mu < 1$ ($\alpha > 180°$): $\bar{\lambda}^4 < 1/\bar{R}\bar{S}$.

(i) Clamped circular edge:

$$C_{11} = J_\mu(\bar{\delta}_1)$$
$$C_{12} = I_\mu(\bar{\delta}_2)$$
$$C_{13} = \pi/2\cdot(\bar{\delta}_1/\bar{\delta}_2)^{\mu}Y_\mu(\bar{\delta}_1)+K_\mu(\bar{\delta}_2)$$
$$C_{14} = 0$$
$$C_{21} = (\sigma_1-1)[\mu J_\mu(\bar{\delta}_1)-\bar{\delta}_1J_{\mu+1}(\bar{\delta}_1)]$$
$$C_{22} = (\sigma_2-1)[\mu I_\mu(\bar{\delta}_2)+\bar{\delta}_2I_{\mu+1}(\bar{\delta}_2)]$$
$$C_{23} = \pi/2\cdot(\sigma_1-1)(\bar{\delta}_1/\bar{\delta}_2)^{\mu}[\mu Y_\mu(\bar{\delta}_1)-\bar{\delta}_1Y_{\mu+1}(\bar{\delta}_1)]+(\sigma_2-1)[\mu K_\mu(\bar{\delta}_2)-\bar{\delta}_2K_{\mu+1}(\bar{\delta}_2)]-\mu(\sigma_1-\sigma_2)(\bar{\delta}_3/\bar{\delta}_2)^{\mu}K_\mu(\bar{\delta}_3)$$
$$C_{24} = -\mu I_\mu(\bar{\delta}_3)$$
$$C_{31} = (\sigma_1-1)\mu J_\mu(\bar{\delta}_1)$$
$$C_{32} = (\sigma_2-1)\mu I_\mu(\bar{\delta}_2)$$
$$C_{33} = \pi/2\cdot(\sigma_1-1)(\bar{\delta}_1/\bar{\delta}_2)^{\mu}\cdot\mu Y_\mu(\bar{\delta}_1)+\mu(\sigma_2-1)K_\mu(\bar{\delta}_2)-(\sigma_1-\sigma_2)(\bar{\delta}_3/\bar{\delta}_2)^{\mu}[\mu K_\mu(\bar{\delta}_3)-\bar{\delta}_3K_{\mu+1}(\bar{\delta}_3)]$$
$$C_{34} = -[\mu I_\mu(\bar{\delta}_3)+\bar{\delta}_3I_{\mu+1}(\bar{\delta}_3)]$$
$$C_{41} = (\sigma_1-1)\bar{\delta}_1^{\mu}$$
$$C_{42} = (\sigma_2-1)\bar{\delta}_2^{\mu}$$
$$C_{43} = (2\sin\mu\pi)^{-1}(\pi\bar{\delta}_2^{-\mu})\cdot[(\sigma_1-1)\bar{\delta}_1^{2\mu}\cos\mu\pi-(\sigma_2-1)\bar{\delta}_2^{2\mu}+(\sigma_1-\sigma_2)\bar{\delta}_3^{2\mu}]$$
$$C_{44} = -\bar{\delta}_3^{\mu}. \quad \text{(B2)}$$

(ii) Simply supported circular edge: C_{ij} are given by eqns (B2), except for $i = 2$, which are defined as follows:

$$
\begin{aligned}
C_{21} &= (\sigma_1-1)(-\bar{\delta}_1^2 J_\mu(\bar{\delta}_1)+(1-\nu)[\mu(\mu-1)J_\mu(\bar{\delta}_1)+\bar{\delta}_1 J_{\mu+1}(\bar{\delta}_1)]) \\
C_{22} &= (\sigma_2-1)(\bar{\delta}_2^2 I_\mu(\bar{\delta}_2)+(1-\nu)[\mu(\mu-1)I_\mu(\bar{\delta}_2)-\bar{\delta}_2 I_{\mu+1}(\bar{\delta}_2)]) \\
C_{23} &= \pi/2\cdot(\sigma_1-1)(\bar{\delta}_1/\bar{\delta}_2)^\mu(-\bar{\delta}_1^2 Y_\mu(\bar{\delta}_1)+(1-\nu)[\mu(\mu-1)Y_\mu(\bar{\delta}_1)+\bar{\delta}_1 Y_{\mu+1}(\bar{\delta}_1)) \\
&\quad+(\sigma_2-1)(\bar{\delta}_2^2 K_\mu(\bar{\delta}_2)+(1-\nu)[\mu(\mu-1)K_\mu(\bar{\delta}_2)+\bar{\delta}_2 K_{\mu+1}(\bar{\delta}_2)]) \\
&\quad+(\sigma_1-\sigma_2)(\bar{\delta}_3/\bar{\delta}_2)^\mu\cdot(1-\nu)\mu[-(\mu-1)K_\mu(\bar{\delta}_3)+\bar{\delta}_3 K_{\mu+1}(\bar{\delta}_3)] \\
C_{24} &= -(1-\nu)\mu[(\mu-1)I_\mu(\bar{\delta}_3)+\bar{\delta}_3 I_{\mu+1}(\bar{\delta}_3)].
\end{aligned}
\tag{B3}
$$

(iii) Free circular edge: C_{2j} and C_{4j} are defined in eqns (B3) and (B2), respectively. C_{1j} and C_{3j} are defined as follows:

$$
\begin{aligned}
C_{11} &= 2(\sigma_1-1)\mu[(\mu-1)J_\mu(\bar{\delta}_1)-\bar{\delta}_1 J_{\mu+1}(\bar{\delta}_1)] \\
C_{12} &= 2(\sigma_2-1)\mu[(\mu-1)I_\mu(\bar{\delta}_2)+\bar{\delta}_2 I_{\mu+1}(\bar{\delta}_2)] \\
C_{13} &= \pi\mu(\sigma_1-1)(\bar{\delta}_1/\bar{\delta}_2)^\mu[(\mu-1)Y_\mu(\bar{\delta}_1)-\bar{\delta}_1 Y_{\mu+1}(\bar{\delta}_1)] \\
&\quad+2(\sigma_2-1)\mu[(\mu-1)K_\mu(\bar{\delta}_2)-\bar{\delta}_2 K_{\mu+1}(\bar{\delta}_2)] \\
&\quad-(\sigma_1-\sigma_2)(\bar{\delta}_3/\bar{\delta}_2)^\mu\cdot[2\mu(\mu-1)K_\mu(\bar{\delta}_3)+\bar{\delta}_3^2 K_\mu(\bar{\delta}_3)+2\bar{\delta}_3 K_{\mu+1}(\bar{\delta}_3)] \\
C_{14} &= -[2\mu(\mu-1)I_\mu(\bar{\delta}_3)+\bar{\delta}_3^2 I_\mu(\bar{\delta}_3)-2\bar{\delta}_3 I_{\mu+1}(\bar{\delta}_3)] \\
C_{31} &= \sigma_1[\mu J_\mu(\bar{\delta}_1)-\bar{\delta}_1 J_{\mu+1}(\bar{\delta}_1)] \\
C_{32} &= \sigma_2[\mu I_\mu(\bar{\delta}_2)+\bar{\delta}_2 I_{\mu+1}(\bar{\delta}_2)] \\
C_{33} &= \pi/2\cdot\sigma_1(\bar{\delta}_1/\bar{\delta}_2)^\mu[\mu Y_\mu(\bar{\delta}_1)-\bar{\delta}_1 Y_{\mu+1}(\bar{\delta}_1)]+\sigma_2[\mu K_\mu(\bar{\delta}_2)-\bar{\delta}_2 K_{\mu+1}(\bar{\delta}_2)]-(\sigma_1-\sigma_2)(\bar{\delta}_3/\bar{\delta}_2)^\mu\cdot[\mu K_\mu(\bar{\delta}_3)] \\
C_{34} &= -\mu I_\mu(\bar{\delta}_3).
\end{aligned}
\tag{B4}
$$

$\bar{\lambda}^4 > 1/\overline{RS}$.

(i) Clamped circular edge:

$$
\begin{aligned}
C_{11} &= J_\mu(\bar{\delta}_1) \\
C_{12} &= J_\mu(\bar{\delta}_2) \\
C_{13} &= -(\bar{\delta}_1/\bar{\delta}_2)^\mu Y_\mu(\bar{\delta}_1)+Y_\mu(\bar{\delta}_2) \\
C_{14} &= 0 \\
C_{21} &= (\sigma_1-1)[\mu J_\mu(\bar{\delta}_1)-\bar{\delta}_1 J_{\mu+1}(\bar{\delta}_1)] \\
C_{22} &= (\sigma_2-1)[\mu J_\mu(\bar{\delta}_2)-\bar{\delta}_2 J_{\mu+1}(\bar{\delta}_2)] \\
C_{23} &= -(\sigma_1-1)(\bar{\delta}_1/\bar{\delta}_2)^\mu[\mu Y_\mu(\bar{\delta}_1)-\bar{\delta}_1 Y_{\mu+1}(\bar{\delta}_1)]+(\sigma_2-1)[\mu Y_\mu(\bar{\delta}_2)-\bar{\delta}_2 Y_{\mu+1}(\bar{\delta}_2)]-\mu(\sigma_1-\sigma_2)(\bar{\delta}_3/\bar{\delta}_2)^\mu Y_\mu(\bar{\delta}_3) \\
C_{24} &= -\mu J_\mu(\bar{\delta}_3) \\
C_{31} &= (\sigma_1-1)\mu J_\mu(\bar{\delta}_1) \\
C_{32} &= (\sigma_2-1)\mu J_\mu(\bar{\delta}_2) \\
C_{33} &= -\mu(\sigma_1-1)(\bar{\delta}_1/\bar{\delta}_2)^\mu\cdot Y_\mu(\bar{\delta}_1)+\mu(\sigma_2-1)Y_\mu(\bar{\delta}_2)-(\sigma_1-\sigma_2)(\bar{\delta}_3/\bar{\delta}_2)^\mu[\mu Y_\mu(\bar{\delta}_3)-\bar{\delta}_3 Y_{\mu+1}(\bar{\delta}_3)] \\
C_{34} &= -[\mu J_\mu(\bar{\delta}_3)-\bar{\delta}_3 J_{\mu+1}(\bar{\delta}_3)] \\
C_{41} &= (\sigma_1-1)\bar{\delta}_1^\mu \\
C_{42} &= (\sigma_2-1)\bar{\delta}_2^\mu \\
C_{43} &= \cot\mu\pi\cdot\bar{\delta}_2^{-\mu}\cdot[-(\sigma_1-1)\bar{\delta}_1^{2\mu}+(\sigma_2-1)\bar{\delta}_2^{2\mu}-(\sigma_1-\sigma_2)\bar{\delta}_3^{2\mu}] \\
C_{44} &= -\bar{\delta}_3^\mu.
\end{aligned}
\tag{B5}
$$

(ii) Simply supported circular edge: C_{ij} are given by eqns (B5), except for $i = 2$, which are as follows:

$$
\begin{aligned}
C_{21} &= (\sigma_1-1)(-\bar{\delta}_1^2 J_\mu(\bar{\delta}_1)+(1-\nu)[\mu(\mu-1)J_\mu(\bar{\delta}_1)+\bar{\delta}_1 J_{\mu+1}(\bar{\delta}_1)]) \\
C_{22} &= (\sigma_2-1)(-\bar{\delta}_2^2 J_\mu(\bar{\delta}_2)+(1-\nu)[\mu(\mu-1)J_\mu(\bar{\delta}_2)+\bar{\delta}_2 J_{\mu+1}(\bar{\delta}_2)]) \\
C_{23} &= -(\sigma_1-1)(\bar{\delta}_1/\bar{\delta}_2)^\mu(-\bar{\delta}_1^2 Y_\mu(\bar{\delta}_1)+(1-\nu)[\mu(\mu-1)Y_\mu(\bar{\delta}_1)+\bar{\delta}_1 Y_{\mu+1}(\bar{\delta}_1)]) \\
&\quad+(\sigma_2-1)(-\bar{\delta}_2^2 Y_\mu(\bar{\delta}_2)+(1-\nu)[\mu(\mu-1)Y_\mu(\bar{\delta}_2)+\bar{\delta}_2 Y_{\mu+1}(\bar{\delta}_2)]) \\
&\quad+(\sigma_1-\sigma_2)(\bar{\delta}_3/\bar{\delta}_2)^\mu\cdot(1-\nu)\mu[-(\mu-1)Y_\mu(\bar{\delta}_3)+\bar{\delta}_3 Y_{\mu+1}(\bar{\delta}_3)] \\
C_{24} &= (1-\nu)\mu[-(\mu-1)J_\mu(\bar{\delta}_3)+\bar{\delta}_3 J_{\mu+1}(\bar{\delta}_3)].
\end{aligned}
\tag{B6}
$$

(iii) Free circular edge: C_{2j} and C_{4j} are defined in eqns (B6) and (B5), respectively. C_{1j} and C_{3j} are defined as follows:

$$C_{11} = 2(\sigma_1-1)\mu[(\mu-1)J_\mu(\bar{\delta}_1)-\bar{\delta}_1 J_{\mu+1}(\bar{\delta}_1)]$$
$$C_{12} = 2(\sigma_2-1)\mu[(\mu-1)J_\mu(\bar{\delta}_2)-\bar{\delta}_2 J_{\mu+1}(\bar{\delta}_2)]$$
$$\begin{aligned} C_{13} = &-2\mu(\sigma_1-1)(\bar{\delta}_1/\bar{\delta}_2)^\mu[(\mu-1)Y_\mu(\bar{\delta}_1)-\bar{\delta}_1 Y_{\mu+1}(\bar{\delta}_1)] \\ &+2(\sigma_2-1)\mu[(\mu-1)Y_\mu(\bar{\delta}_2)-\bar{\delta}_2 Y_{\mu+1}(\bar{\delta}_2)] \\ &-(\sigma_1-\sigma_2)(\bar{\delta}_3/\bar{\delta}_2)^\mu\cdot[2\mu(\mu-1)Y_\mu(\bar{\delta}_3)-\bar{\delta}_3^2 Y_\mu(\bar{\delta}_3)+2\bar{\delta}_3 Y_{\mu+1}(\bar{\delta}_3)] \end{aligned}$$
$$C_{14} = -2\mu(\mu-1)J_\mu(\bar{\delta}_3)+\bar{\delta}_3^2 J_\mu(\bar{\delta}_3)-2\bar{\delta}_3 J_{\mu+1}(\bar{\delta}_3)$$
$$C_{31} = \sigma_1[\mu J_\mu(\bar{\delta}_1)-\bar{\delta}_1 J_{\mu+1}(\bar{\delta}_1)]$$
$$C_{32} = \sigma_2[\mu J_\mu(\bar{\delta}_2)-\bar{\delta}_2 J_{\mu+1}(\bar{\delta}_2)]$$
$$C_{33} = -\sigma_1(\bar{\delta}_1/\bar{\delta}_2)^\mu[\mu Y_\mu(\bar{\delta}_1)-\bar{\delta}_1 Y_{\mu+1}(\bar{\delta}_1)]+\sigma_2[\mu Y_\mu(\bar{\delta}_2)-\bar{\delta}_2 Y_{\mu+1}(\bar{\delta}_2)]-\mu(\sigma_1-\sigma_2)(\bar{\delta}_3/\bar{\delta}_2)^\mu\cdot Y_\mu(\bar{\delta}_3)$$
$$C_{34} = -\mu J_\mu(\bar{\delta}_3). \tag{B7}$$

For $\mu > 1$ ($\alpha < 180°$): This case is *a propos* to all sectorial plate vibration modes when $\alpha > 180°$, and to those modes having one or more radial node lines when $180° < \alpha < 360°$. As previously shown, $B_{n_1} = B_{n_2} = B_{n_3} = 0$, and thus, the sixth order determinants reduce to third order ones (i.e. $\det[C_{ij}] = 0$, $i, j = 1, 2, 3$).

$\bar{\lambda}^4 < 1/\overline{RS}$.

(i) Clamped circular edge:

$$\begin{aligned} C_{11} &= J_\mu(\bar{\delta}_1) \\ C_{12} &= I_\mu(\bar{\delta}_2) \\ C_{13} &= 0 \\ C_{21} &= (\sigma_1-1)[\mu J_\mu(\bar{\delta}_1)-\bar{\delta}_1 J_{\mu+1}(\bar{\delta}_1)] \\ C_{22} &= (\sigma_2-1)[\mu I_\mu(\bar{\delta}_2)+\bar{\delta}_2 I_{\mu+1}(\bar{\delta}_2)] \\ C_{23} &= -\mu I_\mu(\bar{\delta}_3) \\ C_{31} &= (\sigma_1-1)\mu J_\mu(\bar{\delta}_1) \\ C_{32} &= (\sigma_2-1)\mu I_\mu(\bar{\delta}_2) \\ C_{33} &= -[\mu I_\mu(\bar{\delta}_3)+\bar{\delta}_3 I_{\mu+1}(\bar{\delta}_3)]. \end{aligned} \tag{B8}$$

(ii) Simply supported circular edge: C_{ij} are given by eqns (B8), except for $i = 2$, which are defined as follows:

$$\begin{aligned} C_{21} &= (\sigma_1-1)\{-\bar{\delta}_1^2 J_\mu(\bar{\delta}_1)+(1-\nu)[\mu(\mu-1)J_\mu(\bar{\delta}_1)+\bar{\delta}_1 J_{\mu+1}(\bar{\delta}_1)]\} \\ C_{22} &= (\sigma_2-1)\{\bar{\delta}_2^2 I_\mu(\bar{\delta}_2)+(1-\nu)[\mu(\mu-1)I_\mu(\bar{\delta}_2)-\bar{\delta}_2 I_{\mu+1}(\bar{\delta}_2)]\} \\ C_{23} &= -(1-\nu)\mu[(\mu-1)I_\mu(\bar{\delta}_3)+\bar{\delta}_3 I_{\mu+1}(\bar{\delta}_3)]. \end{aligned} \tag{B9}$$

(iii) Free circular edge: C_{2j} are defined in eqns (B9). C_{1j} and C_{3j} are defined as follows:

$$\begin{aligned} C_{11} &= 2(\sigma_1-1)\mu[(\mu-1)J_\mu(\bar{\delta}_1)-\bar{\delta}_1 J_{\mu+1}(\bar{\delta}_1)] \\ C_{12} &= 2(\sigma_2-1)\mu[(\mu-1)I_\mu(\bar{\delta}_2)+\bar{\delta}_2 I_{\mu+1}(\bar{\delta}_2)] \\ C_{13} &= -[2\mu(\mu-1)I_\mu(\bar{\delta}_3)+\bar{\delta}_3^2 I_\mu(\bar{\delta}_3)-2\bar{\delta}_3 I_{\mu+1}(\bar{\delta}_3)] \\ C_{31} &= \sigma_1[\mu J_\mu(\bar{\delta}_1)-\bar{\delta}_1 J_{\mu+1}(\bar{\delta}_1)] \\ C_{32} &= \sigma_2[\mu I_\mu(\bar{\delta}_2)+\bar{\delta}_2 I_{\mu+1}(\bar{\delta}_2)] \\ C_{33} &= -\mu I_\mu(\bar{\delta}_3). \end{aligned} \tag{B10}$$

$\bar{\lambda}^4 > 1/\overline{RS}$.

The elements of the vanishing third order determinants, $\det[C_{ij}] = 0$ $(i,j = 1, 2, 3)$, corresponding to the clamped, simply supported, and free circular edge conditions in this case are identical to those given by eqns (B5)–(B7), except for $j = 3$, where $C_{i3} = C_{i4}$ $(i = 1, 2, 3)$ in eqns (B5)–(B7).

APPENDIX C: INVESTIGATION OF SINGULARITIES OF VIBRATORY BENDING MOMENT AND SHEAR FORCE

Previous work detailing an analytical solution for free vibrations of classically thin sectorial plates having simply supported radial edges (Huang *et al.*, 1992) has concluded that the vibratory bending moments in the region of the vertex ($r = 0$) vary as $r^{\mu-2}$ for $1 \leqslant \mu \leqslant 2$ ($90° < \alpha \leqslant 180°$) and $r^{-\mu}$ for $0 < \mu < 1$ ($\alpha > 180°$). These singular stress orders are identical to those associated with the static biharmonic functions derived by Williams (1952). The intent here is to investigate the order of singularity in the vibratory bending moments and shear forces at the vertex of thick (Mindlin) sectorial plates with simply supported radial edges. In these plates, the strength of the singularities increases with the sector angle, mainly due to the abrupt change of direction of the simply supported radial edges.

Consider the four cases: Case I(a): $\mu \geqslant 1$, $\delta_1^2 > 0$, $\delta_2^2 > 0$, $\delta_3^2 > 0$; Case I(b): $\mu \geqslant 1$, $\delta_1^2 > 0$, $\delta_2^2 < 0$, $\delta_3^2 < 0$; Case II(a): $0 < \mu < 1$, $\delta_1^2 > 0$, $\delta_2^2 > 0$, $\delta_3^2 > 0$; and Case II(b): $0 < \mu < 1$, $\delta_1^2 > 0$, $\delta_2^2 < 0$, $\delta_3^2 < 0$.

Case I(a) : $\mu \geqslant 1, \delta_1^2 > 0, \delta_2^2 > 0, \delta_3^2 > 0$; ($\lambda^4 > 1/RS$)

Since $B_{n_1} = B_{n_2} = B_{n_3} = 0$, eqns (12) and (36) yield the exact solution for free vibration as

$$\phi_1(r,\theta) = A_{n_1} J_\mu(\delta_1 r) \sin \mu\theta \tag{C1}$$

$$\phi_2(r,\theta) = A_{n_2} J_\mu(\delta_2 r) \sin \mu\theta \tag{C2}$$

$$\phi_3(r,\theta) = A_{n_3} J_\mu(\delta_3 r) \cos \mu\theta. \tag{C3}$$

Consider first the radial vibratory bending moment given by eqn (3a). Let $\bar{M}_r$ be the quantity in the bracket of eqn (3a) evaluated at time (t) and along a radial line (θ = constant). Then, substituting eqns (6) and (C1)–(C3) into (3a) yields

$$\begin{aligned}\bar{M}_r = A_{n_1}(\sigma_1-1)(\delta_1^2 J_\mu''(\delta_1 r)+(v/r)[\delta_1 J_\mu'(\delta_1 r)-(\mu^2/r)J_\mu(\delta_1 r)])\\ +A_{n_2}(\sigma_2-1)(\delta_2^2 J_\mu''(\delta_2 r)+(v/r)[\delta_2 J_\mu'(\delta_2 r)-(\mu^2/r)J_\mu(\delta_2 r)])\\ +A_{n_3}[(1-v)/r]((\mu/r)J_\mu(\delta_3 r)-\mu\delta_3 J_\mu'(\delta_3 r)).\end{aligned} \tag{C4}$$

By substituting eqn (21a) into (C4), and performing the indicated differentiations, one finds that all terms of r with order larger than zero vanish in the limit. Thus

$$\lim_{r\Rightarrow 0}\bar{M}_r = \lim_{r\Rightarrow 0}[(1-v)\mu(\mu-1)((\sigma_1-1)(\delta_1/2)^\mu A_{n_1}+(\sigma_2-1)(\delta_2/2)^\mu A_{n_2}-(\delta_3/2)^\mu A_{n_3})r^{\mu-2}/\Gamma(\mu+1)]. \tag{C5}$$

Clearly, the radial bending moment, M_r in the proximity of the vertex ($r = 0$) varies as $r^{\mu-2}$.

Consider now the radial vibratory shear force given by eqn (3d). Let $\bar{Q}_r$ be the quantity in the bracket of the radial shear force eqn (3d) evaluated at time (t) and along radial line (θ = constant). By employing eqn (6), the second regularity condition [eqn (15b)], and the solution eqn (C1), the following limit on $\bar{Q}_r$ as r goes to zero holds

$$\begin{aligned}\lim_{r\Rightarrow 0}\bar{Q}_r &= \lim_{r\Rightarrow 0}(\psi_r \partial W/\partial r)_{\theta=\text{constant}}\\ &= \text{finite value} + \lim_{r\Rightarrow 0}[A_{n_1}\delta_1 J_\mu'(\delta_1 r)+A_{n_2}\delta_2 J_\mu'(\delta_2 r)].\end{aligned} \tag{C6}$$

Utilizing eqns (17) and (24), the limit eqn (C6) approaches a finite value.

Case I(b) : $\mu \geqslant 1, \delta_1^2 > 0, \delta_2^2 < 0, \delta_3^2 < 0$; ($\lambda^4 < 1/RS$)

In this case, the ordinary Bessel functions J_μ, in eqns (C2) and (C3) are simply replaced by modified Bessel functions I_μ. Following the same limiting procedure given in the previous Case I(a), one also finds that near $r = 0$ M_r varies as $\mu-2$. Similarly, for the radial shear force (Q_r), $J_\mu'(\delta_2 r)$ in eqn (C6) are replaced by $I_\mu'(\delta_2 r)$. When eqns (17) and (24) are substituted in the result, $\bar{Q}_r$ is finite in the limit as r goes to zero.

Case II(a) : $0 < \mu < 1, \delta_1^2 > 0, \delta_2^2 > 0, \delta_3^2 > 0$; ($\lambda^4 > 1/RS$)

The exact solution in this case is given by eqns (12) and (36) with the relationship between the integration constants given by eqns (38), (41) and (42). Substituting these into the radial bending moment (M_r) [eqn (3a)] and using eqns (19a), (21a), (41) and (42), one can derive the following limit equation

$$\begin{aligned}\lim_{r\Rightarrow 0}\bar{M}_r = \lim_{r\Rightarrow 0}[(1-v)(\mu-1)((\sigma_1-1)(\mu-2)\delta_1^{2-\mu}B_{n_1}+(\sigma_2-1)(\mu-2)\delta_2^{2-\mu}B_{n_2}\\ +\mu\delta_3^{2-\mu}B_{n_3})(r/2)^{-\mu}/[4\sin\mu\pi\cdot\Gamma(-\mu+2)]].\end{aligned} \tag{C7}$$

Substituting eqns (43) and (44) into (51) yields

$$\begin{aligned}\lim_{r\Rightarrow 0}\bar{M}_r = \lim_{r\Rightarrow 0}[B_{n_2}(1-v)(\mu-1)\delta_2^{-\mu}((\mu-2)[-(\sigma_1-1)\delta_1^2+(\sigma_2-1)\delta_2^2]\\ +(\sigma_1-\sigma_2)\mu\delta_3^2)(r/2)^{-\mu}/[4\sin\mu\pi\cdot\Gamma(-\mu+2)]].\end{aligned} \tag{C8}$$

It is apparent from eqn (C8) that in the neighborhood of $r = 0$, M_r varies as $r^{-\mu}$.

Using eqns (12), (36), (41) and (42), the following limit equation is obtained for $\bar{Q}_r$ [eqn (3d)]

$$\lim_{r\Rightarrow 0}\bar{Q}_r = \text{finite value} + \lim_{r\Rightarrow 0}[A_{n_1}\delta_1 J_\mu'(\delta_1 r)+B_{n_1}\delta_1 Y_\mu'(\delta_1 r)+A_{n_2}\delta_2 J_\mu'(\delta_2 r)+B_{n_2}\delta_2 Y_\mu'(\delta_2 r)]. \tag{C9}$$

The above is expanded further through the use of eqns (17), (19), (21) and (24)

$$\begin{aligned}\lim_{r\Rightarrow 0}\bar{Q}_r = \text{finite value} + \tfrac{1}{2}\lim_{r\Rightarrow 0}[(\delta_1^\mu A_{n_1}+\delta_2^\mu A_{n_2})(r/2)^{\mu-1}[\Gamma(\mu)]^{-1}\\ +\delta_1(\cot(\mu-1)\pi\cdot(\delta_1 r/2)^{\mu-1}[\Gamma(\mu)]^{-1}+\operatorname{cosec}(\mu+1)\pi\cdot(\delta_1 r/2)^{-\mu-1}[\Gamma(-\mu)]^{-1})B_{n_1}\\ +\delta_2(\cot(\mu-1)\pi\cdot(\delta_2 r/2)^{\mu-1}[\Gamma(\mu)]^{-1}+\operatorname{cosec}(\mu+1)\pi\cdot(\delta_2 r/2)^{-\mu-1}[\Gamma(-\mu)]^{-1})B_{n_2}].\end{aligned} \tag{C10}$$

Substituting eqn (43) into (54) yields

$$\lim_{r\Rightarrow 0}\bar{Q}_r = \text{finite value} + \tfrac{1}{2}\lim_{r\Rightarrow 0}[(r/2)^{\mu-1}[\Gamma(\mu)]^{-1}(\delta_1^{\mu}A_{n_1}+\delta_2^{\mu}A_{n_2}+\cot\mu\pi\cdot\delta_2^{-\mu}(-\delta_1^{2\mu}+\delta_2^{2\mu})B_{n_2})]. \quad \text{(C11)}$$

Clearly, $\bar{Q}_r$ in the region of the vertex ($r = 0$) varies as $r^{\mu-1}$.

Case II(b): $0 < \mu < 1$, $\delta_1^2 > 0$, $\delta_2^2 < 0$, $\delta_3^2 < 0$; ($\lambda^4 < 1/\mathrm{RS}$)

In this case, the exact solutions given by eqns (12) and (16) are substituted into the radial moment (M_r) [eqn (6a)]. By simplifying the result through eqns (19), (21), (28) and (30), and performing a limiting process analogous to that outlined in Case II(a), the findings are that M_r varies as $r^{-\mu}$ near $r = 0$. For the radial shear force (Q_r) [eqn (6d)], the solution eqns (12) and (16) along with (31) are used to establish a limit relation on $\bar{Q}_r$ analogous to eqn (C11). As in Case II(a), $\bar{Q}_r$ varies $r^{\mu-1}$ near $r = 0$.

By the same manner, it can be shown that the circumferential bending moment (M_θ), twisting moment ($M_{r\theta}$), and circumferential shear force (Q_θ) varies in r near the vertex as those findings for M_r and Q_r in Cases I(a), I(b), II(a) and II(b).

In summary, the strength of the moment and shear force singularities at the vertex of thick (Mindlin) sectorial plates having simply supported radial edges is independent of the plate thickness (h). This is contrary to what one might expect from the three-dimensional physical sense of a thick sectorial plate, but it is however, what one should derive from the two-dimensional mathematical models, such as Mindlin and classical thin plate theories. The bending moments at the vertex ($r = 0$) of Mindlin sectorial plates varies identically to those occurring in classical thin ones, namely $r^{-\mu}$ for $0 < \mu < 1$ and $r^{\mu-2}$ for $1 < \mu < 2$. If one utilizes the analytical solution for the vibrations of sectorial thin plates with simply supported radial edges (Huang *et al.*, 1992), one is able to find that the shear forces near $r = 0$ vary according to $r^{-(\mu+1)}$ when $0 < \mu < 1$ ($\alpha > 180°$), and $r^{\mu-3}$ when $\mu \geqslant 1$ ($\alpha \leqslant 180°$). In contrast, the shear forces near $r = 0$ of thick sectorial plates vary as $r^{\mu-1}$ when $0 < \mu < 1$. For $\mu \geqslant 1$, no singular shear forces exist at the vertex of thick sectorial plates. Of course, the singular shear forces contribute to the potential energy of thick (Mindlin) sectorial plates, whereas such forces are absent in the potential energy of classically thin sectorial plates.